ISSN 2096-7071 (Print)
ISSN 2096-3101 (Online)
CN 10-1629/R1

CHINA CDC WEEKLY

Vol. 7 No. 4 Jan. 24, 2025

CCDC weekly

中国疾病预防控制中心周报

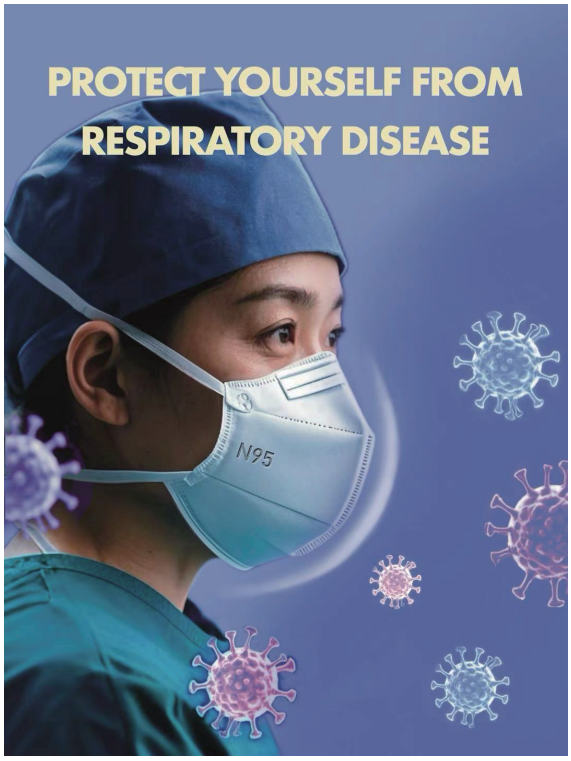

INFECTIOUS DISEASE ISSUE

ISSN 2096-7071
9 772096 707255 04>

Cover Image: credited from the designer Jiaying Wang.

Vital Surveillances

Respiratory Pathogen Profiles of Patients — Beijing Municipality, China, November 2023–April 2024

Han Du[1,&]; Jun Li[2,&]; Haoyu Wen[3,4,&]; Zhixia Gu[5]; Yufei Chang[5]; Wenwan Rong[3,4]; Zhuo Yang[5]; Rahat Ullah Khan[3,4]; Zhaomin Feng[6]; Quanyi Wang[6]; Rui Song[2,#]; Yuhai Bi[1,3,4,#]

ABSTRACT

Introduction: Respiratory pathogens pose a complex challenge for public health systems. In the winter of 2023, multiple respiratory pathogens showed staggered epidemic waves. Additionally, co-infections involving various pathogens were observed, resulting in significant disease burdens. Understanding the epidemiological dynamics of these pathogens is essential for supporting public health systems in the prevention and control of respiratory infectious diseases.

Methods: Respiratory samples were collected from patients in Beijing presenting with influenza-like symptoms to detect 27 respiratory pathogens using multiplex qPCR.

Results: Four distinct epidemic waves were identified. The first wave was a pre-winter outbreak of *Mycoplasma pneumoniae* (*M. pneumoniae*). This was then followed by successive waves of influenza A and B viruses. Severe acute respiratory syndrome coronavirus 2 (SARS-CoV-2) exhibited a resurgence by the end of February 2024. Age-dependent susceptibility varied, with SARS-CoV-2 and influenza A/B peaking in the 30-40-year age group. Conversely, adenovirus, rhinovirus, *M. pneumoniae*, *Moraxella catarrhalis* (*M. catarrhalis*), and *Haemophilus influenzae* (*H. influenzae*) were more common in adolescents and the elderly. Furthermore, 18.8% of cases were identified as co-infections with more than two pathogens. *H. influenzae* was found to frequently co-infect with viral and bacterial pathogens.

Conclusions: Respiratory pathogens exhibited different prevalence trends during the first influenza season following the COVID-19 pandemic. Influenza viruses showed a higher peak incidence and delayed seasonality. Moreover, the co-circulation of viral and bacterial infections increased the complexity of respiratory infections. Interestingly, staggered epidemic waves between SARS-CoV-2 and influenza A/B viruses were observed. Consequently, SARS-CoV-2 may become a seasonal virus, causing epidemics alongside influenza viruses. However, further research is needed to elucidate its epidemiological patterns. The co-circulation of these epidemic viruses and other respiratory pathogens underscores the need for enhanced diagnostic and intervention strategies, including vaccination campaigns.

Entering the first winter after the World Health Organization (WHO) declared coronavirus disease 2019 (COVID-19) no longer a Public Health Emergency of International Concern (PHEIC), an increase in acute respiratory infections caused by multiple respiratory pathogens resulted in increased hospitalizations. This rise in respiratory infections, particularly delayed pediatric *Mycoplasma pneumoniae* (*M. pneumoniae*), among specific age groups differed from typical seasonal patterns (*1*). These changes may be due to the immunity gap developed during the COVID-19 pandemic (*2*). This study investigated the current epidemiological trends of respiratory pathogens in Beijing, with a specific focus on pathogen composition. The findings, combined with global health recommendations, can offer valuable insights for addressing the ongoing challenges posed by respiratory infections in the future.

METHODS

Specimen Source

Oropharyngeal swabs, nasopharyngeal swabs, and sputum samples were collected from patients presenting with respiratory symptoms, including fever, cough, sore throat, shortness of breath, and other influenza-like symptoms. Samples were collected at Ditan Hospital, Haidian Hospital, and surrounding communities in Beijing from November 15, 2023, to

early April 2024. The inclusion criteria consisted of individuals exhibiting at least one of the specified influenza-like symptoms and seeking medical care at the designated locations.

Pathogens Detection

Total DNA/RNA was extracted from 200 μL of sample transport medium containing each patient biospecimen using the MagaBio Pathogens DNA/RNA Purification Kit (Catalog No. BSC75; BIOER) according to the manufacturer's instructions.

In total, 27 common respiratory pathogens were detected here, including severe acute respiratory syndrome coronavirus 2 (SARS-CoV-2), influenza viruses (IAV-IDV), human bocavirus (HBoV), human parainfluenza virus (HPIV-I-IV), respiratory syncytial virus (RSV), adenovirus (ADV), human metapneumovirus (HMPV), human rhinovirus (HRV), human coronaviruses (HCoV-NL63, HCoV-229E, HCoV-OC43, and HCoV-HKU1), and the bacterial pathogens *Klebsiella pneumoniae* (*K. pneumoniae*), *Streptococcus pneumoniae* (*S. pneumoniae*), *Staphylococcus aureus* (*S. aureus*), *Legionella pneumophila* (*L. pneumophila*), *H. influenzae*, *Pseudomonas aeruginosa* (*P. aeruginosa*), *Acinetobacter baumannii* (*A. baumannii*), *M. pneumoniae*, and *M. catarrhalis*, via multiplex quantitative PCR (qPCR) using specific primers, probes, and the detection kit (Influenza A virus, Influenza B virus, and SARS-CoV-2 Triple-Detection Kit, Catalog No. SKY-82130) (*3*). Lab-confirmed cases were defined as those with positive qPCR detection for the different pathogens.

Statistical Analysis

Statistical analyses were performed using R (version 4.3.2). Descriptive statistics, including means, medians, and percentages, summarized the study population characteristics. Chi-square tests compared categorical variables, such as gender, pathogen detection rates between males and females, and differences in pathogen detection rates between hospital and community samples. Correlation analysis assessed interactions between different pathogens. The restricted cubic spline (RCS) method modeled the nonlinear relationship between age and the risk of pathogen occurrence. Multivariable logistic regression models, adjusting for confounders such as age, gender, and clinical symptoms, identified factors associated with pathogen positivity. All statistical analyses were conducted to ensure the reliability and validity of the results, and findings were reported alongside 95% confidence intervals (*CI*s). A $P<0.05$ was considered statistically significant.

RESULTS

Epidemic Characteristics of the Respiratory Pathogens

Between November 2023 and April 2024, a total of 1,513 samples were collected from patients with respiratory tract infections from 2 sentinel hospitals (1,437) and surrounding communities (76) in Beijing. Of these samples, 770 were from male patients, and 743 were from female patients, resulting in a male-to-female ratio of 1.04:1.00. The positive rate for both males and females ($\chi^2=0.84$, $P=0.40$), as well as for hospital and community settings ($\chi^2=3.53$, $P=0.06$), did not show a significant difference. Additionally, there were 158 cases in children (<18 years old) and 1,355 cases in adults (≥18 years old), with a median age of 32 years. Among the collected samples, 787 (52.02%) tested positive for viruses. This included 429 cases (28.35%) of influenza virus infections, with 237 cases (55.24%) of IBV, 190 cases (44.29%) of IAV, and 2 cases (0.47%) of ICV. There were also 150 cases (9.91%) of SARS-CoV-2, 102 cases (6.74%) of HBoV, 72 cases (4.76%) of RSV, 42 cases (2.78%) of ADV, 20 cases (1.32%) of HMPV, and 13 cases (0.86%) of HRV infections. Regarding bacterial infections in patients with fever, 565 cases (37.34%) tested positive for bacteria. The highest detection rate was for *H. influenzae*, accounting for 15.07% of cases. The positive rates for other bacteria are shown in Table 1.

Based on prevalence trends of dominant pathogens, this period can be divided into four epidemic waves: the pre-winter *M. pneumoniae* outbreak with declining SARS-CoV-2 prevalence (Wave 1), followed by the emergence of the IAV epidemic from October to the end of December 2023 (Wave 2), in which the 5.41% detection rate of SARS-CoV-2 was lower than during the COVID-19 pandemic. In contrast to the pathogen prevalence at the end of 2023, the detection rate of IBV increased rapidly and became the dominant pathogen in early 2024 (Wave 3), reaching 34.73%, and then gradually decreased in early February. By mid-February 2024, SARS-CoV-2 infections began to rise, reaching a peak detection rate of 39.04% in mid-March, then gradually decreasing in April, with the number of outpatients with respiratory diseases decreasing significantly (Wave 4, Figure 1). These four

TABLE 1. The number of positive cases and the percentage of 27 respiratory pathogens identified by qPCR in outpatients.

Pathogen type	Pathogen name	Wave 2 (%)	Wave 3 (%)	Sum (%)
Viruses	SARS-CoV-2	42 (5.41)	35 (6.36)	77 (5.81)
	Influenza A virus	170 (21.91)	19 (3.45)	189 (14.25)
	Influenza B virus	27 (3.48)	191 (34.73)	218 (16.44)
	Influenza C virus	1 (0.13)	1 (0.18)	2 (0.15)
	Influenza D virus	0	0	0
	Human bocavirus	49 (6.31)	47 (8.55)	96 (7.24)
	Human metapneumovirus	5 (0.64)	11 (2.00)	16 (1.21)
	Respiratory syncytial virus	36 (4.64)	29 (5.27)	65 (4.90)
	Adenovirus	22 (2.84)	15 (2.73)	37 (2.79)
	Human rhinovirus	10 (1.29)	1 (0.18)	11 (0.83)
	Human parainfluenza virus I	22 (2.84)	48 (8.73)	70 (5.28)
	Human parainfluenza virus II	0	0	0
	Human parainfluenza virus III	4 (0.52)	2 (0.36)	6 (0.45)
	Human parainfluenza virus IV	7 (0.90)	0	7 (0.53)
	Human coronavirus NL63	0	0	0
	Human coronavirus 229E	10 (1.29)	0	10 (0.75)
	Human coronavirus OC43	2 (0.26)	0	2 (0.15)
	Human coronavirus HKU1	1 (0.13)	0	1 (0.08)
Bacterial	*Klebsiella pneumoniae*	67 (8.63)	32 (5.82)	99 (7.45)
	Streptococcus pneumoniae	65 (8.38)	31 (5.64)	96 (7.24)
	Staphylococcus aureus	50 (6.44)	13 (2.36)	63 (4.75)
	Legionella pneumophilia	1 (0.13)	0	1 (0.08)
	Haemophilus influenzae	123 (15.85)	71 (12.91)	194 (14.63)
	Pseudomonas aeruginosa	50 (6.44)	27 (4.91)	77 (5.81)
	Acinetobacter baumannii	53 (6.83)	16 (2.91)	69 (5.20)
	Moraxella catarrhalis	19 (2.45)	6 (1.09)	25 (1.89)
	Mycoplasma pneumoniae	25 (3.22)	8 (1.45)	33 (2.49)

Note: Wave 2 spans from October 10 to December 25, 2023, while Wave 3 extends from December 25, 2023 to February 10, 2024.
Abbreviation: SARS-CoV-2=severe acute respiratory syndrome coronavirus 2; qPCR=quantitative polymerase chain reaction.

waves, each with a different dominant pathogen, highlight the dynamic nature of pathogen prevalence and emphasize the importance of continuous monitoring.

Co-infection Patterns of the Respiratory Pathogens

Of the 1,513 cases of respiratory pathogen infection, 284 (18.77%) were co-infected with more than two respiratory pathogens. Among these, *H. influenzae* was frequently co-infected with other viral and bacterial pathogens (66 cases, 4.36%), followed by IBV (64 cases, 4.23%) and IAV (40 cases, 2.64%). Notably, 18 cases (1.19%) were co-infected by two viruses, including 13 cases of IAV/IBV and HBoV and 5 cases of HBoV and HPIV-I (Figure 2). Correlation analysis revealed potential interactions and impact patterns among these pathogens (Figure 3). A significant negative correlation was found between SARS-CoV-2 and influenza viruses, particularly IBV (P<0.0001). *H. influenzae* was more likely to co-infect with other pediatric-prevalent pathogens, such as ADV (P<0.05), HMPV (P<0.05), and HRV (P<0.0001), but exhibited a significant negative correlation with SARS-CoV-2 (P<0.0001). Additionally, *M. catarrhalis* showed positive correlations with coronaviruses, including SARS-CoV-2 (P<0.0001) and HCoV-229E (P<0.0001). Furthermore, HBoV and HPIV-I showed a significant positive correlation. Interestingly, influenza A and B viruses had a relatively low likelihood of co-infection with other respiratory viruses.

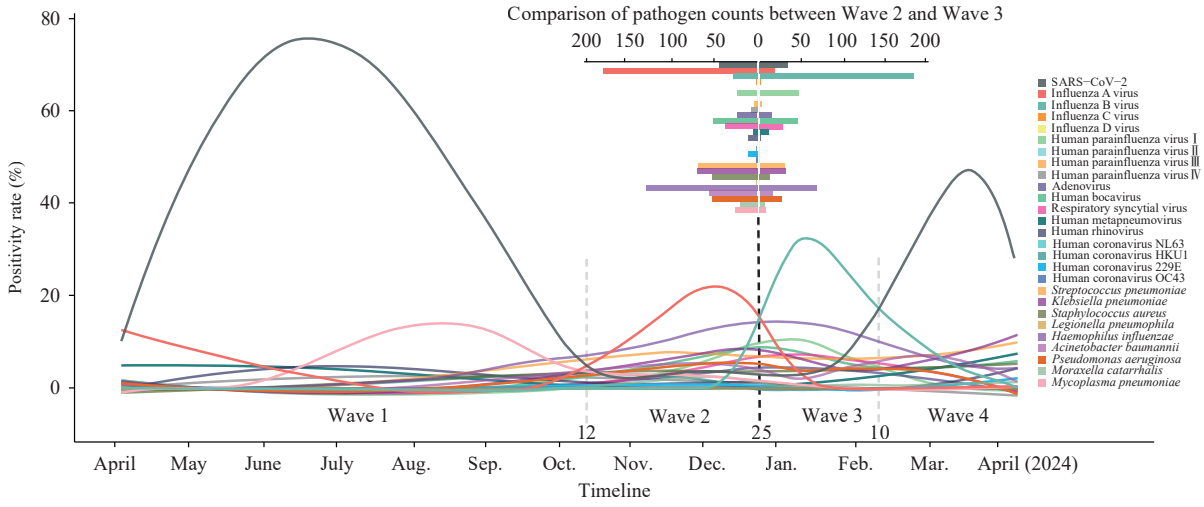

FIGURE 1. Epidemic trend of each pathogen detected by qPCR (November 2023 to April 2024).
Note: This graph depicts the epidemic trend of various pathogens detected by qPCR from November 2023 to April 2024. Each colorful trajectory represents a different pathogen, with the trends reflecting changes in their detected levels over time. The graph's mirrored layout, with an axis on 25 December, facilitates a comparison of trends in Wave 2 and Wave 3. In the upper right, the bar graph details the distribution of detection count for each pathogen during the study period.
Abbreviation: SARS-CoV-2=severe acute respiratory syndrome coronavirus 2; qPCR=quantitative polymerase chain reaction.

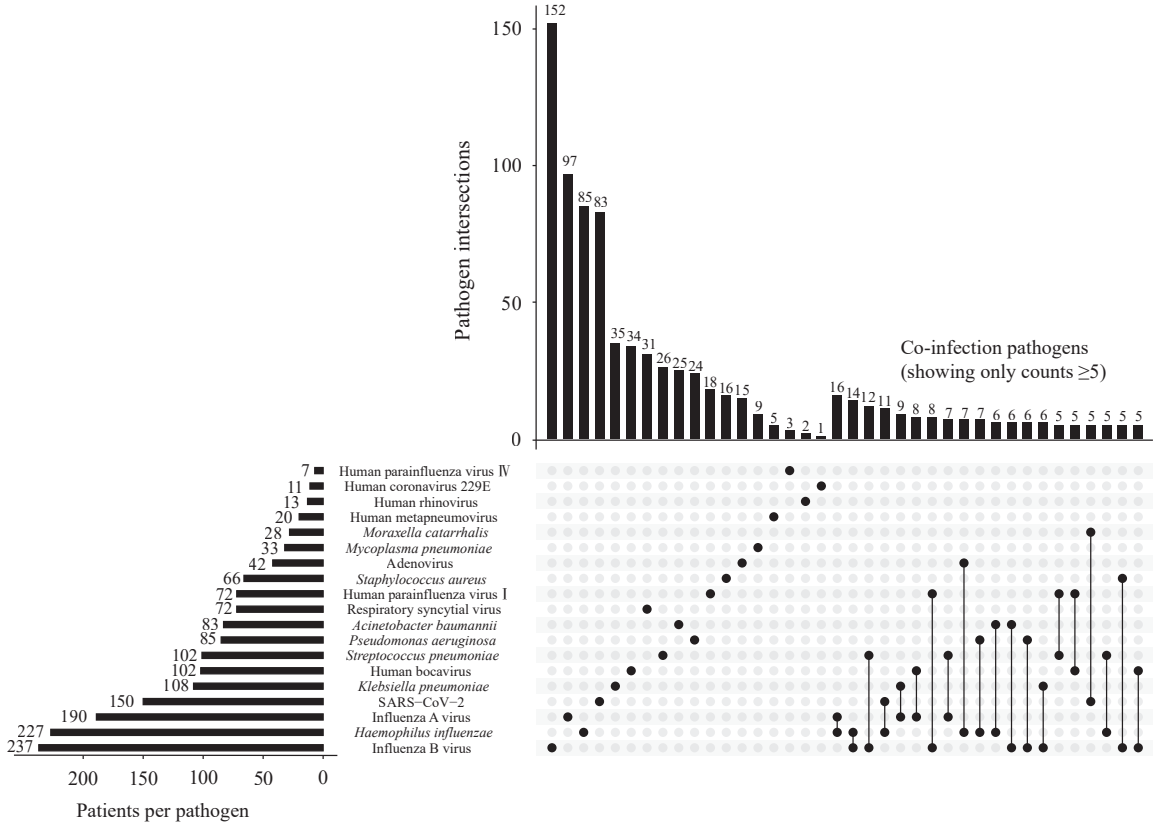

FIGURE 2. Overview of single and co-infections with different pathogens in Beijing (November 2023 to April 2024).
Note: The figure illustrates the co-infection patterns of various pathogens. The horizontal bars represent the total number of infections for each pathogen. The vertical bars display the distribution of infections observed, including both single infections (each circle) and co-infections (linked circles). Only co-infections involving at least five cases are shown.
Abbreviation: SARS-CoV-2=severe acute respiratory syndrome coronavirus 2.

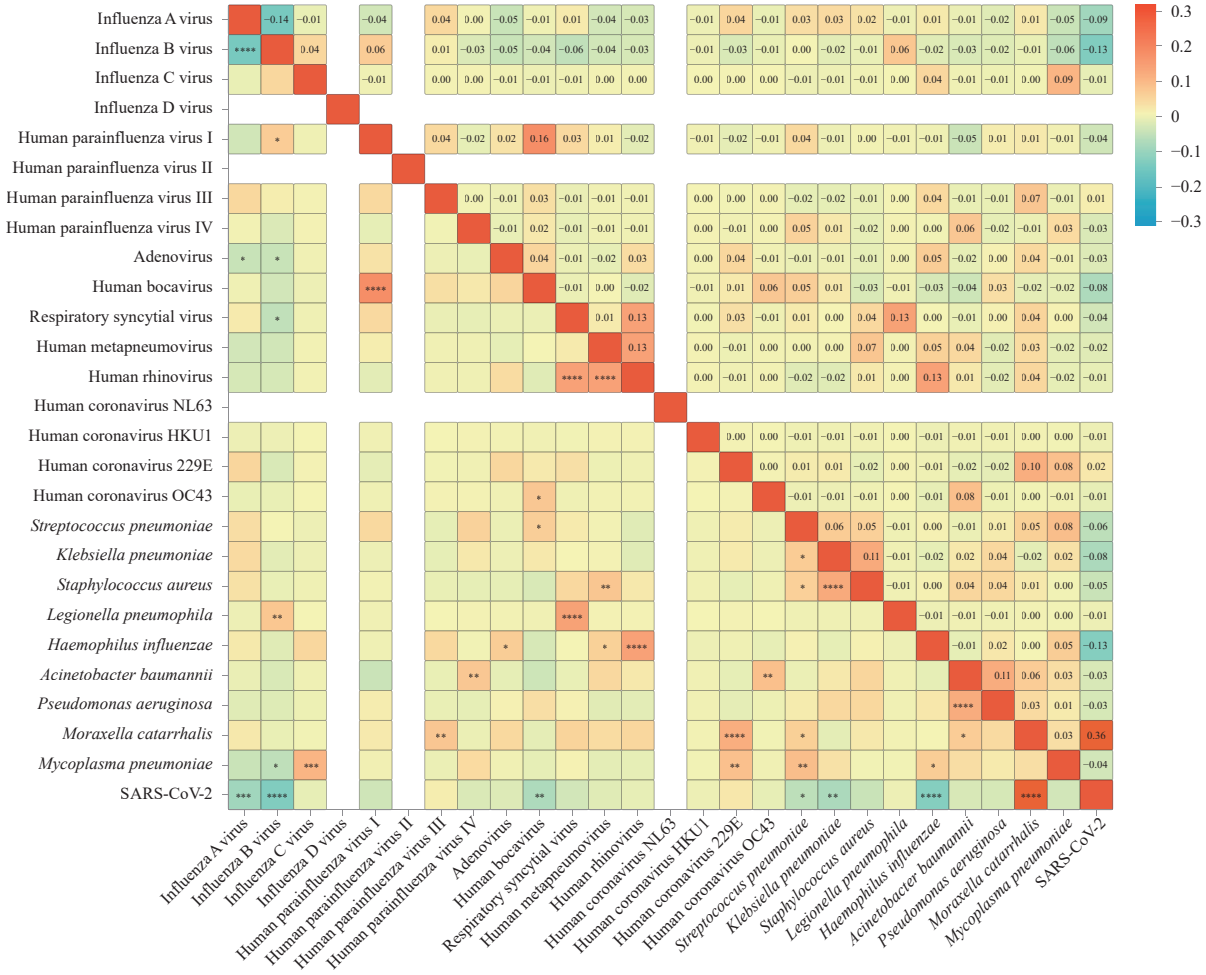

FIGURE 3. Co-infection and correlation among different pathogens in Beijing (November 2023-April 2024).
Note: The heatmap depicts the co-infection and correlation patterns among various pathogens. The color intensity in each cell represents the correlation coefficient between pairs of pathogens: red for positive correlation and blue for negative correlation, with darker shades indicating stronger relationships. The presence of asterisks within the cells denotes statistical significance.
Abbreviation: SARS-CoV-2=severe acute respiratory syndrome coronavirus 2.
* P<0.05;
** P<0.01;
*** P<0.001;
**** P<0.0001.

Age Distribution of the Respiratory Pathogens

The nonlinear relationship between respiratory pathogens and outpatient age was modeled and visualized using RCS. This analysis revealed a significant nonlinear relationship between age and pathogen occurrence risk, with particularly pronounced changes in hazard ratios (*HR*) observed at certain age intervals (Figure 4). Generally, the infection risk profiles of SARS-CoV-2 (Figure 4A), IAV (Figure 4B), and IBV (Figure 4C) exhibited a similar pattern. Susceptibility gradually increased in patients under 30 years old, peaked in the 30–40-year age group, and then decreased. However, unlike SARS-CoV-2 and IAV, which mainly infected middle-aged and elderly individuals, IBV primarily infected middle-aged individuals, with the infection risk rapidly declining after 40 years old. In contrast, *H. influenzae* (Figure 4H) showed increased susceptibility among adolescents, with a substantial risk decrease as age advanced, ultimately stabilizing. HBoV (Figure 4E), RSV (Figure 4F), *A. baumannii* (Figure 4I), *P. aeruginosa* (Figure 4J), *K. pneumoniae* (Figure 4K), and *S. aureus* (Figure 4L) exhibited a U-shaped relationship with age. Among individuals under 30 years old, the

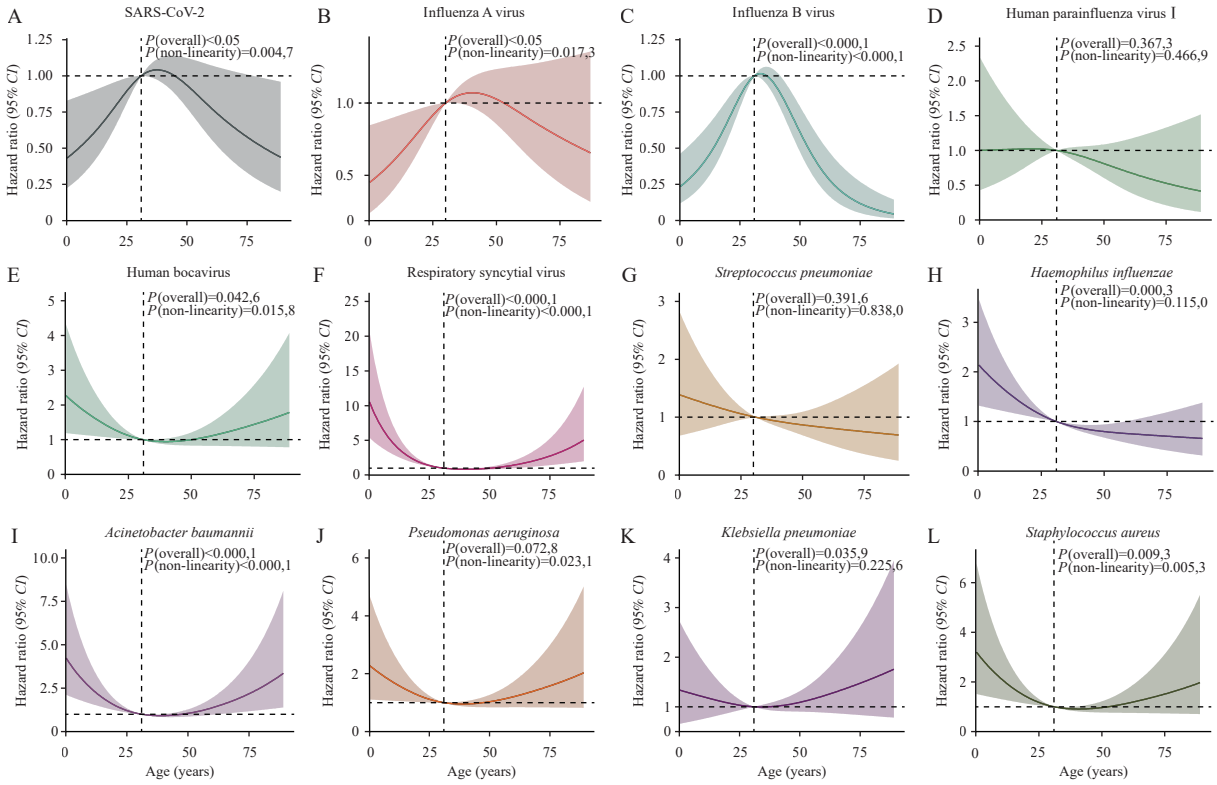

FIGURE 4. Association of respiratory pathogens and the age of outpatients.
Note: The graphs present the nonlinear association analysis between pathogens (counts>50) and age, modeled using the RCS method. Solid lines represent the *HR*s of the influence of age on the occurrence of pathogens, while the shaded areas indicate 95% *CI*s. Knot locations are automatically selected based on the quantiles of age distribution to reveal the nonlinear trend of pathogen risk with age. Additionally, the *P*-values for overall association and nonlinearity are provided for interpretation.
Abbreviation: SARS-CoV-2=severe acute respiratory syndrome coronavirus 2; RCS=restricted cubic spline; *HR*=hazard ratio; *CI*=confidence interval.

risk of infection with these pathogens declined with advancing age, reaching the lowest risk among teenagers and young adults but increasing thereafter with further aging, demonstrating an elevated susceptibility trend among the elderly population. For *S. pneumoniae* (Figure 4G) and other pathogens, the lack of significant nonlinear age-related patterns could be attributable to insufficient statistical power due to sample size limitations or an inherent lack of strong age-dependent susceptibility patterns for these pathogens in the study population.

DISCUSSION

This study focused on pathogen patterns in outpatients with respiratory infections from November 2023 to April 2024. The resurgence of various non-SARS-CoV-2 respiratory pathogens has fluctuated considerably, but the pathogen species remained unchanged. Several epidemic waves occurred, beginning with *M. pneumoniae*, followed by IAV and then IBV. By the end of February 2024, a new wave of SARS-CoV-2 re-emerged and peaked in mid-March. These findings indicate a resurgence of epidemic dynamics for respiratory pathogens from November 2023 to April 2024, with SARS-CoV-2 potentially persisting in long-term circulation in humans, similar to influenza virus and other seasonal pathogens. Notably, SARS-CoV-2 and influenza viruses appeared in staggered epidemic waves, suggesting that immune-mediated interference might cause one virus to diminish during the peak of another, thereby influencing their respective prevalence patterns (*4*). However, the exact epidemic patterns of these pathogens require further monitoring.

Previous studies have shown that multiple respiratory pathogens can easily infect different age groups (*1*). SARS-CoV-2 commonly infects adults, while its detection rate in children is low (*5*), and pediatric infections present with mild, short-lived

symptoms (*6*). The infection risk profiles of IAV and IBV showed a similar pattern to SARS-CoV-2, with susceptibility peaking in the 30–40-year age group. However, a notable increase in pediatric-prevalent pathogens has been observed this winter. It began with a significant outbreak of *M. pneumoniae* among children. As the season progressed, alternating waves of IAV and IBV were observed, leading to a gradual decrease in the risk of infections with HBoV, RSV, *A. baumannii*, *K. pneumoniae*, *S. aureus*, and *P. aeruginosa* in adults. This risk reduction was most pronounced among adolescents and middle-aged adults. However, the risk subsequently increased with advancing age, particularly in the elderly, indicating increased susceptibility in this population.

The data from this study showed that the co-infection of viruses and/or bacteria increased the complexity of respiratory pathogen infections during this epidemic season compared to the COVID-19 pandemic period. The likelihood of co-infection with other respiratory viruses is relatively low for influenza A and B viruses, which may reflect specific host-pathogen interactions or immune responses (*7*). However, there was an elevated risk of secondary bacterial infections following viral respiratory illnesses. Co-infections of viral and bacterial pathogens were important factors that prolonged the infection process, highlighting the need for comprehensive diagnostic approaches to guide effective treatment strategies. In addition to IAV and IBV, other respiratory pathogens, such as RSV, ADV, HRV, and various bacteria, were frequently detected during the epidemic waves. Studies indicate that during influenza epidemics, co-infections involving multiple bacterial species are also common, with nearly 55.6% of severe influenza patients in ICUs experiencing exacerbated conditions due to co-infections with bacteria such as *S. pneumoniae*, *S. aureus*, *M. pneumoniae*, and *H. influenzae* (*8–9*). The rise of antibiotic resistance inevitably makes these co-infections a significant cause of severe pneumonia. In addition, the drug resistance-related genes can also be exchanged among bacteria, which further complicates the treatment. Therefore, co-infection among viruses, as well as between viruses and bacteria, is a major concern (*10*), especially bacteria that show resistance to commonly used antibiotics.

In this study, 27 causative agents for respiratory infections were detected. The results can enhance the understanding of epidemic dynamics and inform effective control strategies. Despite some limitations, such as samples being collected from only 2 sentinel hospitals in the northwest and northeast of Beijing rather than citywide and the relatively small number of pediatric cases, which may introduce bias. Nonetheless, these findings highlight the complexity of respiratory pathogen infections and the importance of comprehensive surveillance.

The alternating epidemics of influenza and SARS-CoV-2 increase the difficulty of prevention and control. The "immunity gap" caused by reduced exposure to common pathogens during prolonged lockdowns may lead to a temporary decline in population immunity, increasing individuals' susceptibility to infections (*2*). This phenomenon underscores the need for strategic vaccination campaigns (*11*), particularly for pathogens that frequently co-infect with other agents, such as influenza (*12*). To reduce the risk of widespread outbreaks, developing more convenient, accurate, and efficient detection methods is crucial. These advancements will significantly improve disease surveillance and control measures in the future.

Conflicts of interest: No conflicts of interest.

Funding: Supported by the National Key R&D Program of China (2023YFC2307500), National Natural Science Foundation of China (82341115 and 32425053), Beijing Research Center for Respiratory Infectious Diseases (BJRID2024-003), National Science and Technology Infrastructure of China (National Pathogen Resource Center-NPRC-32). Youth Innovation Promotion Association of CAS (Y2021034), CAS Project for Young Scientists in Basic Research (YSBR-086), and Innovation Team and Talents Cultivation Program of National Administration of Traditional Chinese Medicine (ZYYCXTD-D-202208).

doi: 10.46234/ccdcw2025.018

[#] Corresponding authors: Rui Song, rui.song@mail.ccmu.edu.cn; Yuhai Bi, beeyh@im.ac.cn.

[1] College of Life Science and Technology, Xinjiang University, Urumchi City, Xinjiang Uygur Autonomous Region, China; [2] Beijing Haidian Hospital, Beijing Haidian Section of Peking University Third Hospital, Beijing, China; [3] CAS Key Laboratory of Pathogen Microbiology and Immunology, Institute of Microbiology, Center for Influenza Research and Early-warning, CAS-TWAS Center of Excellence for Emerging Infectious Diseases, Chinese Academy of Sciences, Beijing, China; [4] University of Chinese Academy of Sciences, Beijing, China; [5] Beijing Ditan Hospital, Capital Medical University, Beijing, China; [6] Beijing Research Center for Respiratory Infectious Diseases, Beijing Center for Disease Prevention and Control, Beijing, China.

[&] Joint first authors.

Submitted: August 29, 2024
Accepted: November 09, 2024
Issued: January 24, 2025

REFERENCES

1. Li ZJ, Zhang HY, Ren LL, Lu QB, Ren X, Zhang CH, et al. Etiological and epidemiological features of acute respiratory infections in China. Nat Commun 2021;12(1):5026. https://doi.org/10.1038/s41467-021-25120-6.
2. Cohen R, Ashman M, Taha MK, Varon E, Angoulvant F, Levy C, et al. Pediatric Infectious Disease Group (GPIP) position paper on the immune debt of the COVID-19 pandemic in childhood, how can we fill the immunity gap? Infect Dis Now 2021;51(5):418-23. http://dx.doi.org/10.1016/j.idnow.2021.05.004.
3. Du H, Du ZT, Wang L, Wang H, Jia MJ, Zhang CG, et al. Fulminant myocarditis induced by SARS-CoV-2 infection without severe lung involvement: insights into COVID-19 pathogenesis. J Genet Genomics 2024;51(6):608 – 16. https://doi.org/10.1016/j.jgg.2024.02.007.
4. Havasi A, Visan S, Cainap C, Cainap SS, Mihaila AA, Pop LA. Influenza A, influenza B, and SARS-CoV-2 similarities and differences - a focus on diagnosis. Front Microbiol 2022;13:908525. https://doi.org/10.3389/fmicb.2022.908525.
5. Kang CK, Shin HM, Park WB, Kim HR. Why are children less affected than adults by severe acute respiratory syndrome coronavirus 2 infection? Cell Mol Immunol 2022;19(5):555-7. http://dx.doi.org/10.1038/s41423-022-00857-2.
6. Wimmers F, Burrell AR, Feng YP, Zheng H, Arunachalam PS, Hu MY, et al. Multi-omics analysis of mucosal and systemic immunity to SARS-CoV-2 after birth. Cell 2023;186(21):4632 – 51.e23. https://doi.org/10.1016/j.cell.2023.08.044.
7. Stowe J, Tessier E, Zhao H, Guy R, Muller-Pebody B, Zambon M, et al. Interactions between SARS-CoV-2 and influenza, and the impact of coinfection on disease severity: a test-negative design. Int J Epidemiol 2021;50(4):1124 – 33. https://doi.org/10.1093/ije/dyab081.
8. Beumer MC, Koch RM, van Beuningen D, OudeLashof AM, van de Veerdonk FL, Kolwijck E, et al. Influenza virus and factors that are associated with ICU admission, pulmonary co-infections and ICU mortality. J Crit Care 2019;50:59 – 65. https://doi.org/10.1016/j.jcrc.2018.11.013.
9. Zhou H, Liu JS, Li LL, Sun J, Wei QJ, Huan Y, et al. Circulation of influenza C virus of C/Sao Paulo/378/82 lineage among pediatric acute respiratory cases, Shandong, China. Virology 2023;587:109855. https://doi.org/10.1016/j.virol.2023.109855.
10. Lu YF, Xue JD, Bi YH. Coinfection and secondary infection of seasonal influenza virus with other pathogens: a review. Acta Microbiol Sin 2022;62(12):4731 – 39. https://doi.org/10.13343/j.cnki.wsxb.20220210.
11. Cohen R, Pettoello-Mantovani M, Somekh E, Levy C. European pediatric societies call for an implementation of regular vaccination programs to contrast the immunity debt associated to coronavirus disease-2019 pandemic in children. J Pediatr 2022;242:260 – 1.e3. https://doi.org/10.1016/j.jpeds.2021.11.061.
12. Yang J, Gong YH, Zhang CG, Sun J, Wong G, Shi WF, et al. Co-existence and co-infection of influenza A viruses and coronaviruses: public health challenges. Innovation (Camb) 2022;3(5):100306. https://doi.org/10.1016/j.xinn.2022.100306.

Vital Surveillances

Characterization of *Aeromonas* Strains Isolated from Adult Patients with Diarrhea and Aquatic Environments — Beijing Municipality, China, 2016–2022

Ying Li[1,&]; Keyi Yu[2,&]; Xiaoli Du[3]; Yuwei Liu[1]; Aixia Yan[1]; Miao Wang[1]; Ying Kang[1]; Shoufei Li[1]; Yuanyuan Wang[1]; Luotong Wang[1]; Shengtian Liu[1]; Tao Peng[1]; Jun Li[4]; Duochun Wang[3]; Zhenzhou Huang[4,#]

ABSTRACT

Introduction: *Aeromonas* is widely distributed in aquatic environments. This study describes the pathogenic characteristics of *Aeromonas* isolated from adult diarrhea patients and aquatic environments in Beijing, China.

Methods: *Aeromonas* isolates from patients with diarrhea and river water samples were assessed using whole-genome sequencing (WGS) and antibiotic resistance profiling.

Results: In total, 38 *Aeromonas* isolates were collected. Among these, 13 isolates were from patients with common clinical symptoms, including diarrhea, abdominal pain, and nausea. Four of 13 *Aeromonas*-positive patients were co-infected with other intestinal pathogens. Patient-derived *Aeromonas* isolates showed high resistance to ampicillin, ampicillin-sulbactam, nalidixic acid, and tetracycline, whereas water-derived isolates showed high resistance to ampicillin, ampicillin-sulbactam, and nalidixic acid. Phylogenetic analysis revealed seven independent branches, without significant clustering among patient- and water-derived isolates.

Conclusions: This study provides valuable insights into the prevalence and characteristics of *Aeromonas*. The intertwined distribution of patient- and water-derived isolates in the phylogenetic tree deserves attention.

The genus *Aeromonas* is widely distributed in aquatic environments and is known to cause various diseases in humans and animals (*1*). These diseases include gastroenteritis, wound infections, bacteremia/sepsis, and immune dysfunction (*2*–*3*). Recently, certain motile *Aeromonas* species have emerged as food- and waterborne pathogens, raising concern (*4*–*5*). Previous studies have reported that a majority (96.5%) of clinical *Aeromonas* isolates are identified as *A. caviae* (29.9%), *A. dhakensis* (26.3%), *A. veronii* (24.8%), and *A. hydrophila* (15.5%) (*4*,*6*). Of these, *A. hydrophila*, *A. caviae*, and *A. veronii* are considered clinically significant (*7*–*8*). *Aeromonas* species cause severe, short-duration diarrheal disease or chronic loose stools, particularly in children, the elderly, and immunocompromised individuals (*9*), as well as traveler's diarrhea (*9*–*10*).

In this study, *Aeromonas* strains were isolated from adult patients with diarrhea and aquatic environments in Beijing Municipality, China. Whole-genome sequencing (WGS) and antibiotic resistance profiling were performed on these *Aeromonas* isolates. The findings of this research will provide valuable insights into the investigation of adult diarrhea caused by *Aeromonas* in Beijing, China.

METHODS

This study enrolled outpatients with acute diarrhea from two clinics in one district of Beijing, China, between January 1, 2016, and December 31, 2022, following the guidelines of the local adult diarrhea surveillance project in Beijing. Acute diarrhea was defined as at least three passages of watery, loose, mucous, or bloody stools within 24 hours. Patient age, sex, occupation, and clinical symptoms were recorded. Fresh fecal samples (5 mg) were collected from each patient, stored in Cary-Blair medium at 4 °C, and transported to the laboratory within 24 hours for bacterial isolation and real-time PCR detection. Additionally, in August 2023, water samples (1 L) were collected from the mainstream of the Chaobai River and its tributaries in Beijing, which flow through the study area. All collection sites were located away from factories and farms. Samples were stored in sterile containers and transported to the laboratory for

Aeromonas isolation within 2 hours.

Stool samples from patients were cultured to isolate various pathogens, including *Aeromonas* spp., *Salmonella*, *Shigella*, diarrheal *Escherichia coli*, *Vibrio parahaemolyticus*, *Vibrio cholerae*, *Campylobacter jejuni*, *Campylobacter coli*, and *Yersinia enterocolitis* (*11*). Real-time PCR was performed for the detection of norovirus, rotavirus, human sapovirus, adenovirus, and astrovirus using corresponding commercial kits (Beijing Applied Biological Technologies Co., Ltd., China). River water samples were cultured to isolate only *Aeromonas* spp. For bacterial isolation, 200 mg of each patient stool sample was inoculated in alkaline peptone water (APW) and enriched at 37 °C for 24 h. Alternatively, 20 mL of 10× APW was added to river water samples and enriched at 37 °C for 24 h. After enrichment, a loopful of culture was streaked on MacConkey (MAC) agar and Rimler-Shotts (RS) agar and incubated at 37 °C for 24 h. Five presumptive *Aeromonas* colonies from the selective agar plate were selected and inoculated in tryptic soy agar (TSA) and incubated at 37 °C for 24 h. Each pure colony culture was initially identified using MALDI-TOF MS (Bruker).

Genomic DNA was extracted using the Wizard Genomic DNA Purification Kit (Promega, Madison, WI, USA) following the manufacturer's instructions. DNA samples (total amount >20 μg) were sent to the Beijing Genomics Institute for next-generation sequencing. The DNA concentration reached 50 ng/μL, and the OD260/280 ratio was 1.8–2.0 for individual samples. Low-quality reads were discarded, and clean data were assembled into genomic contigs using SOAPdenovo version 2.04. After removing contigs shorter than 500 bp, QUAST version 5.0.1 was used to assess the quality of the assembled genomes (Gurevich et al., 2013). Next, Prokka version 1.12 (Seemann, 2014), Prodigal version 2.6.3 (Hyatt et al., 2010), and RAST (https://rast.nmpdr.org/) were used to annotate the genomes. The genome sequences of *Aeromonas* isolates and seven strain types (*A. hydrophila* ATCC 7966T [accession No.: GCA_000014805], *A. caviae* NCTC 12244T [GCA_900476005], *A. dhakensis* TN14 [GCA_905132925], *A. veronii* FDAARGOS_632 [GCA_008693705], *A. media* CECT 4232T [GCA_000819985], *A. sanarellii* LMG 24682T [GCA_000820085], *A. schubertii* ATCC 43700T [GCA_001481395]) were included in this study. ANI analysis was used to determine the evolutionary distance among the bacterial isolates at the genomic level. ANI values >95% were considered indicative of the same species. Prokka version 1.12 and the Roary genome pipeline with an identity cutoff of 95% were used to perform gene annotation and pan-genome analysis, respectively. Snippy was used to identify core genome single nucleotide polymorphisms (cgSNPs), with the genome sequence of *A. hydrophila* ATCC 7966T used as the reference. The phylogenetic evolutionary tree was constructed based on decombined cgSNPs by IQ-TREE using maximum likelihood estimation with 1,000 bootstraps. The genome sequences of the *Aeromonas* strains sequenced in this study have been deposited at GenBank/DDBJ/ENA under the BioProject ID No. PRJNA1097280.

Antimicrobial susceptibility testing (AST) was then performed for *Aeromonas* using a microbroth dilution method and a panel for aerobic, gram-negative bacilli (Shanghai Fosun Long March Medical Science Co., Ltd., China). Antibiotic susceptibility (S), intermediate resistance (I), and resistance (R) were interpreted according to the Clinical and Laboratory Standards Institute (CLSI) guidelines M45A2E (CLSI, 2019). *Escherichia coli* ATCC 25922 was used as a control. The following antimicrobials were tested: ampicillin (AMP), ampicillin-sulbactam (AMS), tetracycline (TET), meropenem (MEM), polymyxin E (CT), ceftazidime/avibactam (CZA), cefotaxime (CTX), ceftazidime-avibactam (CAZ), ciprofloxacin (CIP), chloramphenicol (CHL), nalidixic acid (NAL), streptomycin (STR), sulfamethoxazole tablets (SXT), and amikacin (AMK). *Aeromonas* strains were defined as multidrug-resistant (MDR) if they were resistant to three or more antimicrobial classes.

Statistical analyses were performed using Stata software (version 12.0). The chi-squared test was used to compare isolation rates between groups, with statistical significance set at $P<0.05$.

RESULTS

Distribution of *Aeromonas* in Patients with Diarrhea

A total of 2,011 stool samples were collected from 2,011 patients with diarrhea between January 1, 2016, and December 31, 2022, excluding 2020, due to the COVID-19 pandemic. Of these, 13 *Aeromonas* isolates (S1–S13), identified using MALDI-TOF MS, were derived from 13 patients (P1–P13), resulting in a

positive *Aeromonas* rate of 0.65% (13/2,011). The annual positive rates were 0.27% (1/365) in 2016, 0% (0/371) in 2017, 0.53% (2/374) in 2018, 0.56% (2/358) in 2019, 0.84% (3/359) in 2021, and 2.72% (5/184) in 2022. These isolates were identified by their ANI values as *A. veronii* (*n*=5), *A. caviae* (*n*=5), and *A. dhakensis* (*n*=3; Table 1 and Figure 1). Four of the 13 *Aeromonas*-positive patients were co-infected with other intestinal pathogens: patient P1 with *V. parahaemolyticus* (tdh+/trh-); P2 with *Salmonella* and EAEC; P3 with *V. parahaemolyticus* (tdh+/trh-); and P8 with *V. parahaemolyticus* (tdh+/trh-) and EPEC (Table 1).

Among the 13 *Aeromonas*-positive patients, 7 were male and 6 were female, aged 16 to 81 years. Disease onset occurred in April (*n*=1), June (*n*=3), July (*n*=4), and August (*n*=5; Table 1). In the epidemiological investigation, all 13 patients reported consuming suspected contaminated food products, including cold meat, barbecue, fried food, salad, seafood, cold drinks, and takeaway fast food (Table 1). The most common clinical symptoms were diarrhea (100%, 13/13), abdominal pain (92.30%, 12/13), nausea (61.54%, 8/13), vomiting (23.08%, 3/13), weakness (15.38%, 2/13), dehydration (15.38%, 2/13), and fever (15.38%, 2/13). Moreover, 69.23% (9/13) and 30.77% (4/13) of patients presented with watery and loose stools, respectively (Table 1). Patients P11 and P12 were 2 students from the same school, with the same disease onset time (August 13, 2022). On this day, 5 individuals (including P11 and P12) at this school experienced diarrhea after consuming takeaway fast food delivered by the same catering company. All 5 patients presented with diarrhea (watery stools) and abdominal pain (Table 1).

Ten aquatic environmental samples (named A1–A10) were collected in this study, from which 25 *Aeromonas* isolates were identified using MALDI-TOF MS. One sample (A8) yielded no isolates; the other nine water samples yielded between 1 and 5 *Aeromonas* isolates each. The isolates were further classified as *A. veronii* (*n*=11), *A. caviae* (*n*=9), *A. schubertii* (*n*=2), *A. sanarellii* (*n*=1), *A. dhakensis* (*n*=1), and a species closely related to *A. media* (*n*=1; Table 2 and Figure 1).

Antibiotic Susceptibility of *Aeromonas* Isolates

The *Aeromonas* isolates from patients exhibited high resistance to AMP (92.31%), AMS (84.62%), NAL (69.23%), STR (61.54%), and TET (38.46%). However, fewer than 30% of isolates resisted the other antibiotics. Eight isolates (61.54%, 8/13) were identified as MDR, with the most dominant resistance patterns being AMP+AMS+NAL+STR (15.38%) and AMP+AMS+NAL (15.38%; Table 3 and Figure 2).

The *Aeromonas* isolates from river water samples showed high resistance to AMP (96.00%), AMS (96.00%), NAL (60.00%), and STR (32.00%). Resistance to other antibiotics was observed in less than 30% of isolates. Eleven isolates (44.00%, 11/25) were MDR. The dominant resistance pattern was AMP+AMS (20.00%; Table 3 and Figure 3).

Phylogenetic Analysis of *Aeromonas*

A phylogenetic tree was constructed using cgSNP data from the *Aeromonas* strains with the reference sequence *A. hydrophila* ATCC 7966T (Figure 4). The analysis revealed seven phylogenetic groups with a high bootstrap value. Seven species of *Aeromonas* were located on their respective independent phylogenetic branches. Strains from patients were mainly distributed in the phylogenetic branches of *A. veronii*, *A. caviae*, and *A. dhakensis*, while those from the river water samples were distributed in six different phylogenetic branches other than the *A. hydrophila* branch. Of all *Aeromonas* isolates obtained in this study, two isolates of *A. schubertii* (R6-2 and R9-1) from the river water samples displayed genetic clustering; however, overall, there was no significant clustering observed between the isolates from patients and those from river water samples. The *Aeromonas* isolates from patients, and those from river water samples showed a significant distance between their phylogenetic branches even when they belonged to the same species and were derived from the same water sample. Moreover, the isolates from patients and the aquatic environment of the river water samples were intertwined in the phylogenetic tree.

CONCLUSION

Aeromonas species are recognized enteric pathogens, but their mechanisms of pathogenicity remain unclear. Previous studies from various locations have reported variable rates of *Aeromonas* detection in patients with diarrhea. For instance, a study in Barcelona, Spain, reported a 2.09% (18/863) positive rate of *Aeromonas* in travelers with diarrhea, with *A. veronii* and *A. caviae* as the dominant species (*12*). Another study in Tainan City, Taiwan, China, also identified *A. veronii* and *A. caviae* as the dominant species in fish and clinical

TABLE 1. Information and clinical symptoms of patients with positive isolation of *Aeromonas*.

Patient number	Time of onset	Sex	Age	Clinical symptoms	Suspected contaminated food	Number of people dining together/ co- diners who experienced diarrhea	Bacterial culture results			
							Number of *Aeromonas* isolate	ANI analysis results of *Aeromonas*	ANI value (%)	Other pathogens detected
P1	July 29, 2016	Male	26	Diarrhea (watery stools 10 times per day) + abdominal pain + fever (38.1 ℃)	Barbecue	1/-	S1	*A.caviae*	97.936	*Vibrio parahaemolyticus*[*]
P2	July 16, 2018	Female	30	Diarrhea (watery stools 10 times per day) + abdominal pain + nausea	Cold meat	2/no	S2	*A.dhakensis*	97.2863	*Salmonella*[†] + EAEC
P3	August 10, 2018	Male	44	Diarrhea (watery stools 12 times per day) + abdominal pain + nausea + vomiting	Barbecue	1/-	S3	*A.dhakensis*	97.179	*V. parahaemolyticus*[*]
P4	June 25, 2019	Female	17	Diarrhea (loose stools 10 times per day) + abdominal pain + nausea + dehydration	Fried food	6/yes	S4	*A.caviae*	97.9062	/
P5	July 16, 2019	Female	30	Diarrhea (loose stools 10 times per day) + abdominal pain + nausea	Cold meat	3/no	S5	*A.dhakensis*	97.0422	/
P6	April 23, 2021	Male	81	Diarrhea (watery stools 10 times per day) + abdominal pain + nausea + weak + dehydration + vomiting	Cold meat	1/-	S6	*A.caviae*	97.9036	/
P7	June 3, 2021	Female	20	Diarrhea (loose stools 6 times per day) + abdominal pain + nausea + weak + fever (39.4 ℃)	Salad	1/-	S7	*A.veronii*	96.4188	/
P8	July 26, 2021	Male	38	Diarrhea (watery stools 8 times per day) + abdominal pain + nausea	Seafood	1/-	S8	*A.veronii*	96.5328	*V. parahaemolyticus*[*]+ EPEC
P9	June 13, 2022	Male	40	Diarrhea (watery stools 10 times per day) + abdominal pain + nausea	Cold drink	1/-	S9	*A.caviae*	97.8955	/
P10	August 4, 2022	Male	35	Diarrhea (loose stools 5 times per day) + abdominal pain	Cold meat	3/yes	S10	*A.caviae*	97.9052	/
P11	August 13, 2022	Female	16	Diarrhea (watery stools 7 times per day) + abdominal pain	Take-away fast food[§]	5/yes[¶]	S11	*A.veronii*	96.5436	/
P12	August 13, 2022	Female	17	Diarrhea (watery stools 5 times per day) + abdominal pain	Take-away fast food[§]	5/yes[**]	S12	*A.veronii*	97.4809	/
P13	August 27, 2022	Male	41	Diarrhea (watery stools 6 times per day) + abdominal pain + nausea + vomiting	Cold meat	1/-	S13	*A.veronii*	96.4993	/

Abbreviation: ANI=average nucleotide identity; EAEC=enteroaggregative *Escherichia coli*; EPEC=enteropathogenic *Escherichia coli*
[*] The virulence gene characteristics of *Vibrio parahaemolyticus* are *tdh*+/ *trh*-;
[†] serotype is *Salmonella* Typhimurium;
[§] specific foods include duck meat, chicken meat, broccoli, rice, boiled corn, tomato and egg soup, and apples;
[¶] P12 is one of the five co-diners of P11;
[**] P11 is one of the five co-diners of P12.

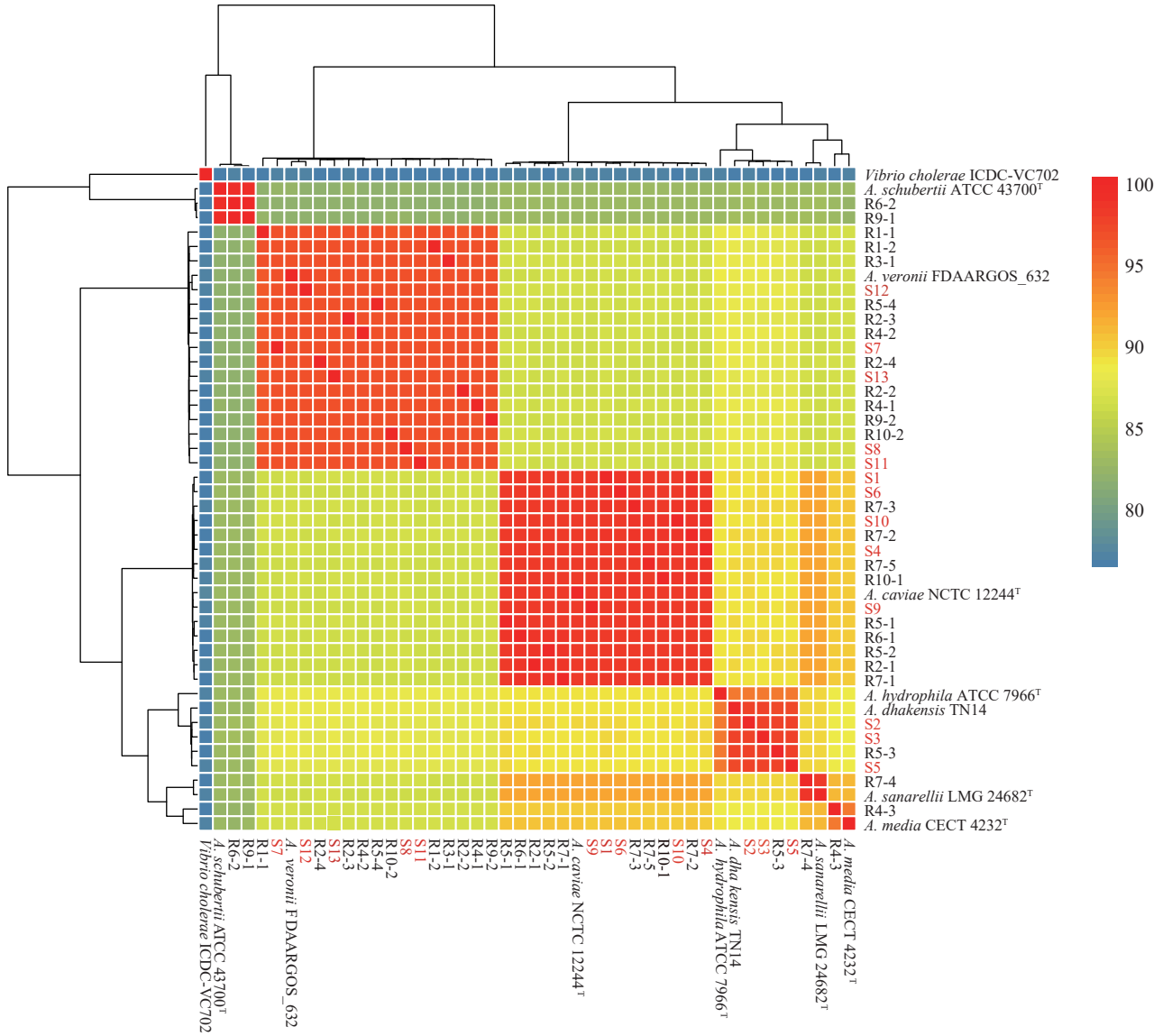

FIGURE 1. Average nucleotide identity analysis of *Aeromonas* isolates.
Note: The red font represents strains from patients with diarrhea. T = type strain.

samples (*13*). Additionally, in Hong Kong Special Adiministrative Region, China, Chan et al. documented a 6.9% incidence of *Aeromonas* in adult patients with acute diarrhea (*13*). Isolation rates of *Aeromonas* from individuals with diarrheal illness in developed countries range from 0.8% to 7.4% (*14*). The most commonly isolated species implicated in gastroenteritis caused by *Aeromonas* include *A. veronii*, *A. hydrophila*, and *A. caviae*, with *A. trota* and *A. jandaei* occurring less frequently (*15*). Similar to the aforementioned studies, our study isolated *Aeromonas* from 13 (0.65%) of the 2,011 patients with diarrhea, with *A. veronii* and *A. caviae* being the most frequently isolated species.

In a previous study, gastroenteritis attributed to *A. sobria* was characterized by acute abdominal pain, vomiting, diarrhea (watery stools), and fever (*16*), similar to the clinical symptoms of the patients enrolled in the present study. All 13 *Aeromonas*-positive patients experienced abdominal pain and diarrhea, with diarrhea occurring 5–12 times per day and characterized by watery or loose stools. This was similar to the symptoms and stool characteristics caused by *V. parahaemolyticus*, a widely distributed pathogenic bacterium in aquatic products (*17*). Although the genus *Aeromonas* was initially considered to belong to the family Vibrionaceae, successive phylogenetic analyses have indicated that *Aeromonas* is not closely related to the genus *Vibrio*, resulting in the reassignment of *Aeromonas* from the family

TABLE 2. Distribution of *Aeromonas* from river water samples.

River water sample	Bacterial culture results	*Aeromonas* isolate	ANI analysis results of *Aeromonas*	ANI value (%)
A1	+	R1-1	*A. veronii*	96.19
		R1-2	*A. veronii*	96.48
A2	+	R2-1	*A. caviae*	97.89
		R2-2	*A. veronii*	96.38
		R2-3	*A. veronii*	96.55
		R2-4	*A. veronii*	96.48
A3	+	R3-1	*A. veronii*	96.48
A4	+	R4-1	*A. veronii*	96.49
		R4-2	*A. veronii*	96.44
		R4-3	Species closely related to *A. media*	94.03
A5	+	R5-1	*A. caviae*	97.82
		R5-2	*A. caviae*	97.94
		R5-3	*A. dhakensis*	97.16
		R5-4	*A. veronii*	96.50
A6	+	R6-1	*A. caviae*	97.88
		R6-2	*A. schubertii*	99.00
A7	+	R7-1	*A. caviae*	97.91
		R7-2	*A. caviae*	97.97
		R7-3	*A. caviae*	97.87
		R7-4	*A. sanarellii*	98.02
		R7-5	*A. caviae*	97.84
A8	−	/	/	/
A9	+	R9-1	*A. schubertii*	98.98
		R9-2	*A. veronii*	96.53
A10	+	R10-1	*A. caviae*	97.83
		R10-2	*A. veronii*	96.40

+: represents the sample culture positive in *Aeromonas*.
−: represents the sample culture negative in *Aeromonas*.
Abbreviation: ANI=average nucleotide identity.

TABLE 3. Results of antibiotic sensitivity test for *Aeromonas* species.

Antibiotic	Diarrhea patient isolates (% P/T)*	River sample isolates (% P/T)
AMP	92.31 (12/13)	96.00 (24/25)
AMS	84.62 (11/13)	96.00 (24/25)
TET	38.46 (5/13)	24.00 (6/25)
MEM	0 (0/13)	12.00 (3/25)
CT	15.38 (2/13)	4.00 (1/25)
ETP	23.08 (3/13)	24.00 (6/25)
CZA	0 (0/13)	0 (0/25)
CTX	0 (0/13)	12.00 (3/25)
CAZ	0 (0/13)	0 (0/25)
CIP	0 (0/13)	0 (0/25)
CHL	7.69 (1/13)	8.00 (2/25)
NAL	69.23 (9/13)	60.00 (15/25)
SXT	23.08 (3/13)	8.00 (2/25)
STR	61.54 (8/13)	32.00 (8/25)
AMK	0 (0/13)	0 (0/25)

Abbreviation: AMP=ampicillin; AMS=ampicillin-sulbactam; TET=tetracycline; MEM=meropenem; CT=polymyxin E; ETP=ertapenem; CZA=ceftazidime/avibactam; CTX=cefotaxime; CIP=ciprofloxacin; NAL=nalidixic acid; CAZ=ceftazidime-avibactam; CHL=chloramphenicol; STR=streptomycin; SXT=Sulfamethoxazole Tablets; AMK=amikacin.
* P=number of resistance isolates; T=total number of isolates.

Vibrionaceae to a new family (*18*). Notably, in the present study, all 13 *Aeromonas*-positive patients reported consuming suspected contaminated food, with cold meat products being the most commonly reported (38.46% of patients). Cold meat products are associated with a high risk of foodborne diseases due to cross-contamination between raw and cooked products, which has also been observed in outbreaks caused by *V. parahaemolyticus* in China (*19–22*). In the present study, *V. parahaemolyticus* was co-detected in 23.08% of *Aeromonas*-positive patients. The similarities between *Aeromonas* and *V. parahaemolyticus* regarding their environmental distribution, association with suspected contaminated food, and clinical symptoms, as well as the co-infection of *Aeromonas* and *V. parahaemolyticus*, warrant further investigation. It is important to note that the subjective nature of patient-reported information about suspicious contaminated food is a limitation of the present study.

Aeromonas spp. are transmitted through food and water, with the ability to survive and, rapidly reproduce at low temperatures, and resist chlorine-containing disinfectants (*23*). However, to date, large-scale foodborne or waterborne outbreaks caused by *Aeromonas* spp. have not been reported (*23*). In the present study, 2 patients (P11 and P12) who dined together and consumed takeout food from the same catering company — along with 3 other individuals — experienced diarrhea symptoms on the same day, suggesting a potential outbreak. However, genomic analysis did not confirm a common clone or establish a clear link between the outbreak and *Aeromonas* spp. Successful molecular tracing of diarrhea outbreaks associated with *Aeromonas* spp. has been limited (*16*,*24–25*). Nevertheless, outbreaks caused by multiple *Aeromonas* spp. in patients have been reported (*26*), indicating a need for additional data on pathogenic characteristics in such outbreaks.

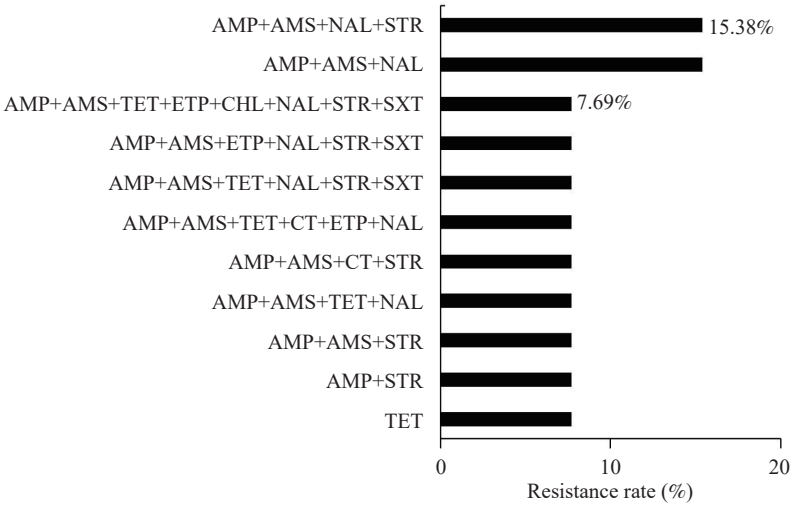

FIGURE 2. Resistance spectrum of 13 strains of *Aeromonas* from patients to various antibiotic combinations.
Note: The X-axis represents the resistance rate of *Aeromonas*. The Y-axis represents a series of antibiotic combinations.

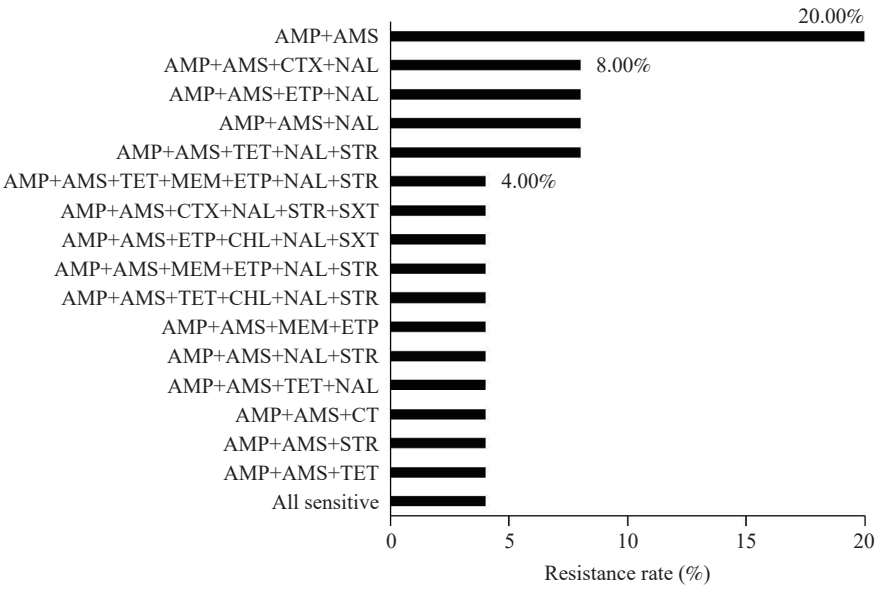

FIGURE 3. Resistance spectrum of 25 strains of *Aeromonas* from river water samples to various antibiotic combinations.
Note: The X-axis represents the resistance rate of *Aeromonas*. The Y-axis represents a series of antibiotic combinations.

In this study, *A. veronii* and *A. caviae* were the dominant species among the 25 *Aeromonas* isolates recovered from environmental water samples. Isolates from both patients and river water exhibited high levels of multidrug resistance, particularly to AMP and AMS. Although not statistically significant, the resistance rates to TET, CT, STR, and SXT — 4 antibiotics commonly used in clinical settings — were slightly higher among isolates from patients than among those from river water. This finding suggests that clinical treatment may contribute to antibiotic resistance in *Aeromonas*.

The high bootstrap values of the main branches in the phylogenetic tree, based on cgSNP analysis of *Aeromonas* isolates from patients and river water samples, indicate a stable and reliable topology. Few isolates clustered significantly, and none were clonal (except for isolates R6-2 and R9-1, identified as *A. schubertii*). Patient-derived isolates of the same *Aeromonas* species (e.g., S7, S8, S11, S12, and S13) and isolates from the same river water sample belonging to the same species (e.g., R7-2, R7-3, and R7-4) were phylogenetically distant, suggesting they did not originate from a recent common ancestor. The interspersed distribution of patient-derived and river water-derived isolates in the phylogenetic tree

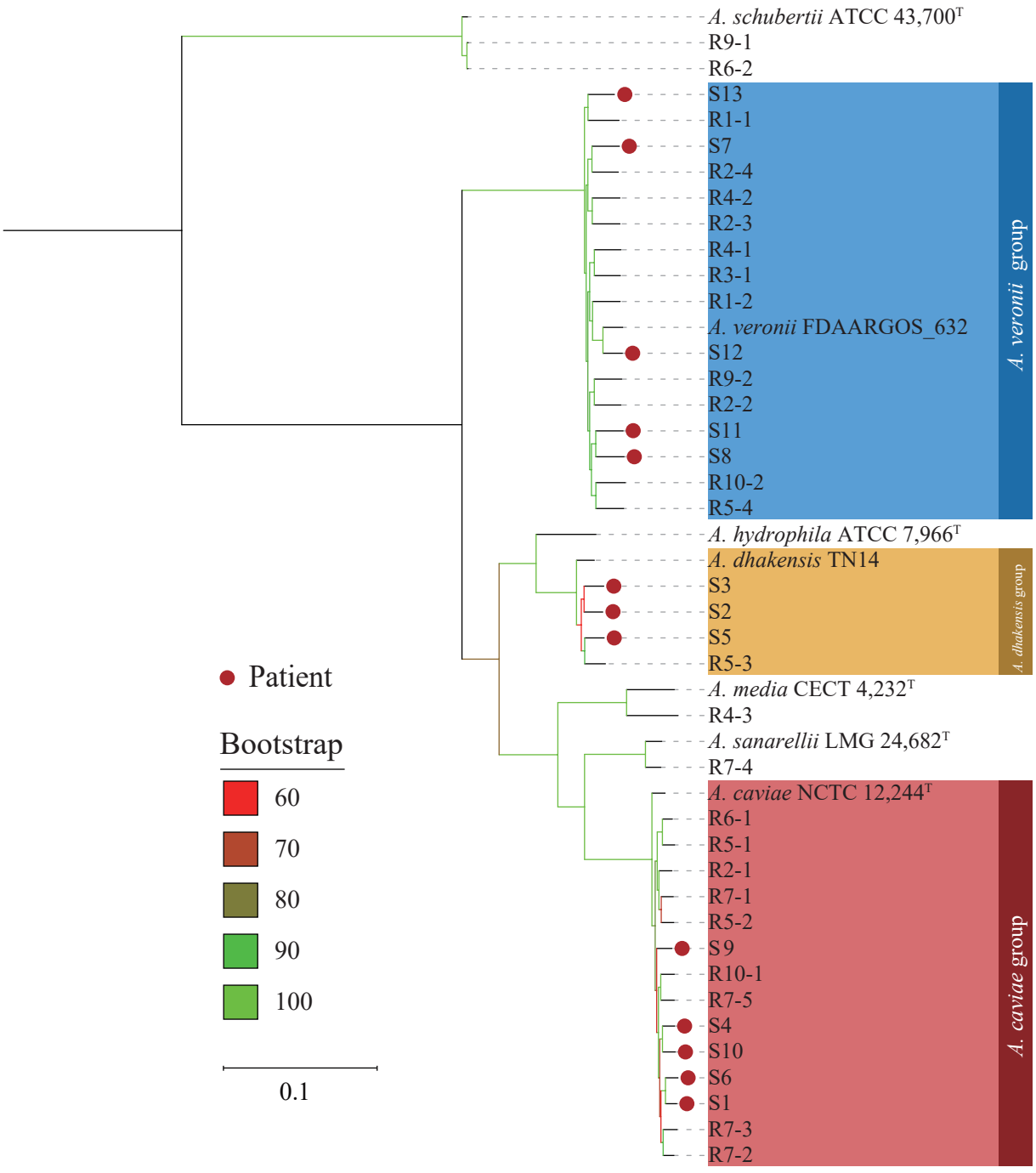

FIGURE 4. Phylogenetic maximum likelihood tree based on core genome single nucleotide polymorphisms among *Aeromonas* strains.
Note: Seven type strains or representative strains were also included. The three largest clusters (*A. veronii*, *A. caviae*, *A. dhakensis*) are shown in blue, red, and yellow, respectively. The red dots on the top of the branches represent *Aeromonas* strains isolated from patients with diarrhea. The various colors of branches (from red to green) represent bootstrap values ranging from 60% to 100%. ^{T} = type strain.

underscores the importance of active surveillance for foodborne pathogens.

This study provides valuable insights into the prevalence and characteristics of *Aeromonas* in patients with diarrhea and aquatic environments. However, the study has limitations, including the subjective nature of patient-reported information and challenges establishing causal links between outbreaks and *Aeromonas*, highlighting areas for further investigation.

Conflicts of interest: No conflicts of interest.

Funding: Supported by the National Key Research Program of China (2021YFF0703801).

doi: 10.46234/ccdcw2025.019

[#] Corresponding author: Zhenzhou Huang, huangzhenzhou@hzcdc.com.cn.

[1] Shunyi District Center for Disease Control and Prevention, Beijing, China; [2] Zhejiang Province Center for Disease Control and Prevention, Hangzhou City, Zhejiang Province, China; [3] National Institute for Communicable Disease Control and Prevention, Chinese Center for Disease Control and Prevention, Beijing, China; [4] Microbiological Laboratory, Hangzhou Center for Disease Control and Prevention (Hangzhou Health Supervision Institution), Hangzhou City, Zhejiang Province, China.
[&] Joint first authors.

Submitted: September 24, 2024
Accepted: November 29, 2024
Issued: January 24, 2025

REFERENCES

1. Ghenghesh KS, Ahmed SF, El-Khalek RA, Al-Gendy A, Klena J. Aeromonas-associated infections in developing countries. J Infect Dev Ctries 2008;2(2):81-98. https://pubmed.ncbi.nlm.nih.gov/19738331/.
2. Figueras MJ, Beaz-Hidalgo R. Aeromonas infections in humans. In: Graf J, editor. Aeromonas. Norfolk: Caister Academic Press. 2015; p. 65-108. http://dx.doi.org/10.21775/9781908230560.04.
3. Janda JM, Abbott SL. The genus *Aeromonas*: taxonomy, pathogenicity, and infection. Clin Microbiol Rev 2010;23(1):35 – 73. https://doi.org/10.1128/CMR.00039-09.
4. Araújo VS, Pagliares VA, Queiroz MLP, Freitas-Almeida AC. Occurrence of *Staphylococcus* and enteropathogens in soft cheese commercialized in the city of Rio de Janeiro, Brazil. J Appl Microbiol 2002;92(6):1172 – 7. https://doi.org/10.1046/j.1365-2672.2002.01656.x.
5. Ansari M, Rahimi E, Raissy M. Antibiotic susceptibility and resistance of *Aeromonas* spp. isolated from fish. Afr J Microbiol Res 2011;5(31):5772 – 5. https://doi.org/10.5897/AJMR11.1240.
6. Latif Eugenín FL. Aeromonas, un microorganismo ambiental de importancia en salud humana y animal [dissertation]. Tarragona: Universitat Rovira i Virgili; 2015. https://dialnet.unirioja.es/servlet/tesis?codigo=78774.
7. Janda JM. Recent advances in the study of the taxonomy, pathogenicity, and infectious syndromes associated with the genus *Aeromonas*. Clin Microbiol Rev 1991;4(4):397 – 410. https://doi.org/10.1128/CMR.4.4.397.
8. Janda JM, Abbott SL. Evolving concepts regarding the genus *Aeromonas*: an expanding panorama of species, disease presentations, and unanswered questions. Clin Infect Dis 1998;27(2):332 – 44. https://doi.org/10.1086/514652.
9. Daskalov H. The importance of *Aeromonas hydrophila* in food safety. Food Control 2006;17(6):474 – 83. https://doi.org/10.1016/j.foodcont.2005.02.009.
10. Vila J, Ruiz J, Gallardo F, Vargas M, Soler L, Figueras MJ, et al. *Aeromonas* spp. and traveler's diarrhea: clinical features and antimicrobial resistance. Emerg Infect Dis 2003;9(5):552 – 5. https://doi.org/10.3201/eid0905.020451.
11. Li Y, Zhang S, He M, Zhang YC, Fu YY, Liang H, et al. Prevalence and molecular characterization of *Campylobacter* spp. isolated from patients with diarrhea in Shunyi, Beijing. Front Microbiol 2018;9:52. https://doi.org/10.3389/fmicb.2018.00052.
12. Chopra AK, Houston CW. Enterotoxins in *Aeromonas*-associated gastroenteritis. Microbes Infect 1999;1(13):1129 – 37. https://doi.org/10.1016/S1286-4579(99)00202-6.
13. Chan SSW, Ng KC, Lyon DJ, Cheung WL, Cheng AFB, Rainer TH. Acute bacterial gastroenteritis: a study of adult patients with positive stool cultures treated in the emergency department. Emerg Med J 2003;20(4):335 – 8. https://doi.org/10.1136/emj.20.4.335.
14. Igbinosa IH, Igumbor EU, Aghdasi F, Tom M, Okoh AI. Emerging *Aeromonas* species infections and their significance in public health. Sci World J 2012;2012:625023. https://doi.org/10.1100/2012/625023.
15. von Graevenitz A. The role of *Aeromonas* in diarrhea: a review. Infection 2007;35(2):59 – 64. https://doi.org/10.1007/s15010-007-6243-4.
16. Taher AAI, Rao BN, Alganay KG, El-Arabi MB. An outbreak of acute gastroenteritis due to *Aeromonas sobria* in Benghazi, Libyan Arab Jamahiriya. East Mediterr Health J 2000;6(2-3):497 – 9. https://doi.org/10.26719/2000.6.2-3.497.
17. Li XY, Shi Y, Wang SM, Dai Y, Huang Q, Chen LL, et al. Analysis on epidemic characteristics of foodborne diseases outbreaks with cross-contamination between raw and cooked food in China's Mainland from 2010 to 2020. Chin J Food Hyg 2022;34(5):1016 – 21. https://doi.org/10.13590/j.cjfh.2022.05.024.
18. Villari P, Crispino M, Montuori P, Boccia S. Molecular typing of *Aeromonas* isolates in natural mineral waters. Appl Environ Microbiol 2003;69(1):697 – 701. https://doi.org/10.1128/AEM.69.1.697-701.2003.
19. Shimohata T, Takahashi A. Diarrhea induced by infection of *Vibrio parahaemolyticus*. J Med Invest 2010;57(3-4):179 – 82. https://doi.org/10.2152/jmi.57.179.
20. Lu J, Wang XL, Wu LH. The progress of foodborne disease prevention and control in the world. Chin J Dis Control Prev 2017;21(2):196 – 9. https://doi.org/10.16462/j.cnki.zhjbkz.2017.02.022.
21. Xiong RR, Liu J, Xu H, Bai L, Pan YJ, Zhao Y, et al. Research progress in mathematical simulation and precise prevention and control strategies for cross-contamination risk of foodborne pathogens. Food Sci 2024;45(14):288 – 98. https://doi.org/10.7506/spkx1002-6630-20230719-200.
22. Bai L, Liu LS, Li LL, Wang YR, Wang YBN, Qi Y, et al. Comparison of foodborne disease outbreaks data in China and the United States from 2011 to 2017 and its inspiration for the construction of monitoring system in China. Chin J Food Hyg 2022;34(5):863 – 70. https://doi.org/10.13590/j.cjfh.2022.05.001.
23. Wadström T, Ljungh Å. *Aeromonas* and *Plesiomonas* as food- and waterborne pathogens. Int J Food Microbiol 1991;12(4):303 – 11. https://doi.org/10.1016/0168-1605(91)90144-e.
24. Taneja N, Khurana S, Trehan A, Marwaha RK, Sharma M. An outbreak of hospital acquired diarrhea due to *Aeromonas sobria*. Indian Pediatr 2004;41(9):912-6. https://pubmed.ncbi.nlm.nih.gov/15475633/.
25. Tsheten T, Tshering D, Gyem K, Dorji S, Wangchuk S, Tenzin T, et al. An outbreak of aeromonas hydrophila food poisoning in Deptsang village, Samdrup Jongkhar, Bhutan, 2016. J Res Health Sci 2016;16(4):224-7. https://pubmed.ncbi.nlm.nih.gov/28087856/.
26. Hofer E, dos Reis CMF, Theophilo GND, Cavalcanti VO, de Lima NV, de Fátima Correia de Miranda Henriques M. Aeromonas associated with an acute diarrhea outbreak in São Bento do Una, Pernambuco. Rev Soc Bras Med Trop 2006;39(2):217 – 20. https://doi.org/10.1590/s0037-86822006000200016.

Preplanned Studies

Epidemiological and Spatiotemporal Clustering Analysis of Human Brucellosis — China, 2019–2023

Zhiguo Liu[1,&]; Yue Shi[2,&]; Chuizhao Xue[3]; Min Yuan[1]; Zhenjun Li[2,#]; Canjun Zheng[2,#]

Summary

What is already known about this topic?

The number of reported cases of human brucellosis significantly increased from 45,046 (3.25/100,000) in 2019 to 70,439 (4.99/100,000) in 2023.

What is added by this report?

Human brucellosis continued to spread and expand of in northern China, with the most cases reported in the Inner Mongolia Autonomous Region (*n*=87,961), Xinjiang Uygur Autonomous Region (*n*=27,845) and Shanxi Province (*n*=21,932). In southern China, reported cases increased substantially from 2,036 in 2019 to 5,128 in 2023. Joinpoint regression analysis revealed an upward trend in incidence rate across 29 provincial-level administrative divisions (PLADs), with an annual percent change (APC) of 12.86, (P<0.05), with particularly rapid increases observed in most southern PLADs. Spatiotemporal analysis identified high-risk clusters concentrated in the northwestern and northeastern regions.

What are the implications for public health practice?

With the continued worsening of human brucellosis over the past five years, implementing strict controls on the movement of infected animals is urgeent.

Brucellosis is a globally significant zoonotic disease that causes substantial economic losses and poses serious occupational health risks (*1*–*2*). Since 1995, brucellosis has reemerged in China, reaching a historic peak in 2014, with the affected areas expanding from northern to southern regions (*3*). Notably, in 2021, 69,767 cases were reported across 2,083 counties in China, representing a 47.7% increase from 2020 (47,425) (*4*). However, epidemiological evolution characteristics of human brucellosis from 2019 to 2023 remain unclear. Therefore, this study aims to analyze disease evolution patterns and to identify high-risk areas for human brucellosis in China from 2019 to 2023.

The case and incidence rates were obtained from the National Notifiable Disease Reporting System (NNDRS) for the period January 1, 2019 to December 31, 2023. The average annual growth rate was calculated according to previously reported methods (*5*). Average annual incidence growth rates (%) were calculated using power functions in Microsoft Excel 2021 (Microsoft Corporation, Redmond, Washington, United States).

The Qinling-Huaihe line served as the geographical boundary between northern and southern China. The northern region comprised 16 provincial-level administrative divisions (PLADs) [Heilongjiang, Jilin, Liaoning, Beijing, Tianjin, Inner Mongolia, Shaanxi, Hebei, Henan, Ningxia, Shanxi, Shandong, Gansu, Qinghai, Xinjiang (Xinjiang Production and Construction Corps, XPCC) and Xizang], while the southern region included 15 PLADs (Jiangsu, Shanghai, Zhejiang, Anhui, Hunan, Hubei, Sichuan, Chongqing, Guizhou, Yunnan, Guangxi, Guangdong, Hainan, Fujian and Jiangxi). Hong Kong Special Administrative Region (SAR); Macau SAR; and Taiwan, China were excluded due to data unavailability.

Joinpoint regression analyses were performed using Joinpoint Regression Program version 5.2.0 (https://surveillance.cancer.gov/joinpoint/) (National Cancer Institute, Bethesda, Maryland, USA) based on Poisson regression to estimate joinpoint positions and regression coefficients (*6*). Annual percentage changes (APCs) were calculated to quantify the year-over-year rate changes between successive joinpoints as percentages.

A retrospective space-time scan analysis using the discrete Poisson model was conducted using SaTScan v10.1.3 (National Cancer Institute, Bethesda, Maryland, USA) to identify spatiotemporal clusters of human brucellosis. Statistical significance was assessed through 999 Monte Carlo simulations. The log likelihood ratio (LLR) test statistic was constructed by comparing observed and expected case counts inside and outside the scanning window. Clusters were defined by scanning windows with statistically

significant LLR values (P<0.05).

From 2019 to 2023, human brucellosis cases and incidence rates demonstrated a fluctuating upward trend across 31 PLADs in China, with 304,668 total reported cases and an average annual incidence of 4.33/10,000 population (Figure 1).

The annual reported cases increased from 45,046 (3.25/100,000) in 2019 to 48,455 (3.45/100,000) in 2020, reaching a peak of 71,628 (5.06/100,000) in 2021. Subsequently, cases slightly decreased to 69,100 (4.89/10,000) in 2022 before rising again to 70,439 (4.99/10,000) in 2023 (Figure 1). Further, 87.78% (267,446/304,668) of cases occurred in northern PLADs, while 12.22% (37,222/304,668) were reported from southern PLADs. Notably, southern PLADs experienced a substantial increase in reported cases, from 4,310 in 2019 to 10,363 in 2023 (Figure 1 and Table 1).

From 2019 to 2023, Inner Mongolia accounted for the largest proportion (87,961 cases; 28.87% of all reports) with an average annual incidence of 71.88/100,000 (Table 1). Shanghai reported the lowest number of cases (22), followed by Hainan (257), with average annual incidence rates of 0.018/100,000 and 0.31/100,000, respectively. With the exception of Yunnan, all southern PLADs reported incidence rates below 1.0/100,000 (Table 1).

The average annual growth rate of incidence in China from 2019 to 2023 was 8.97% (Table 2). Notably, 13 southern PLADs and 5 northern PLADs reported average annual growth rates exceeding 10% (Table 2). Qinghai showed a marked upward trend, with annual incidence increasing from 2.45/100,000 in 2019 to 34.86/100,000 in 2023. Although most southern PLADs maintained incidence rates below 1.0/100,000, they showed consistent increases over time (Table 2).

Joinpoint regression analysis revealed APCs ranging from –0.70 to 97.97, with 29 PLADs demonstrating significant upward trends in incidence rates, except for Jilin and Xizang (Table 3). Notably, six PLADs — Qinghai, Guizhou, Yunnan, Sichuan, Jiangxi, and Guangxi (Table 3) — exhibited particularly significant increases, with five of these PLADs located in southern China.

Retrospective space-time analysis scanning for clusters with high rates using the discrete Poisson model identified 14 distinct zones of human brucellosis clusters. The largest cluster occurred between January 1, 2022, and December 31, 2023, encompassing 419 counties (Figure 2 and Table 3). This primary cluster demonstrated a relative risk of 8.95 with a LLR of 79,182.30 (P<0.001) (Figure 2 and Table 4).

The second largest cluster, comprising 33 counties across Inner Mongolia, Jilin, and Liaoning, was identified between January 1, 2020, and December 31, 2021, with a relative risk of 20.75 and LLR of 40,377.28 (P<0.001) (Figure 2). The third largest cluster included 19 counties in Henan Province during January 1, 2022, to December 31, 2023, exhibiting a relative risk of 3.73 and LLR of 2,140.47 (P<0.001). The remaining 11 clusters each contained 1 to 3 counties, distributed across Henan, Shandong, Yunnan, and Sichuan (Figure 2 and Table 4).

DISCUSSION

Our analysis reveals that human brucellosis continued to spread and expand, the majority of cases remain concentrated in northern China, with PLADs in the northwestern and northeastern region. Inner Mongolia's cases, accounting for 28.87% of the national total, indicate ineffective control measures and inadequate containment of animal brucellosis (*7*). In

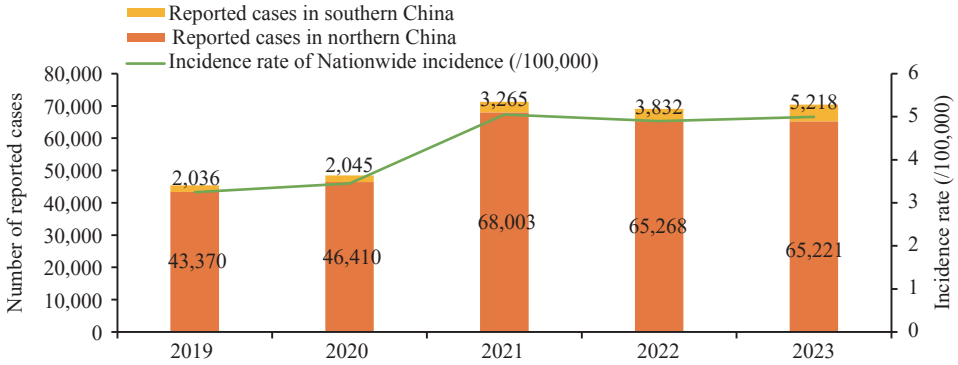

FIGURE 1. Evolution trend of human brucellosis in northern and southern China, from 2019 to 2023.

TABLE 1. Number of reported cases in 31 PLADs in China from 2019 to 2023.

Areas	PLADs	Number of reported cases, 2019-2023					Total cases
		2019	2020	2021	2022	2023	
Northern	Inner Mongolia	14,148	16,406	21,910	19,088	16,409	87,961
	Xinjiang	4,135	3,079	4,828	6,469	9,334	27,845
	Shanxi	3,465	3,498	4,962	4,876	5,131	21,932
	Ningxia	2,242	2,988	5,049	6,295	4,505	21,079
	Henan	2,274	3,121	5,032	5,254	5,145	20,826
	Gansu	1,787	3,003	4,601	5,229	5,569	20,189
	Hebei	3,407	3,158	4,777	3,970	4,196	19,508
	Liaoning	2,298	3,000	5,483	3,916	3,162	17,859
	Heilongjiang	4,326	2,956	4,119	2,849	3,387	17,637
	Shandong	2,534	2,427	3,370	3,218	3,311	14,860
	Shaanxi	1,138	1,116	1,419	1,705	1,543	6,921
	Jilin	1,191	1,151	1,311	847	1,093	5,593
	Qinghai	148	259	772	1,159	2,074	4,412
	Tianjin	136	136	238	258	209	977
	Beijing	86	54	83	115	131	469
	Xizang	55	58	49	20	22	204
Southern	Yunnan	321	383	701	1,039	1,519	3,963
	Guangdong	456	361	479	490	612	2,398
	Anhui	142	229	353	347	414	1,485
	Hunan	212	167	239	248	349	1,215
	Jiangsu	142	165	284	284	299	1,174
	Sichuan	114	130	206	267	417	1,134
	Guangxi	153	125	229	248	367	1,122
	Fujian	151	111	195	207	238	902
	Zhejiang	108	127	181	209	195	820
	Hubei	80	73	107	175	254	689
	Guizhou	33	54	92	140	207	526
	Jiangxi	58	53	103	80	177	471
	Chongqing	49	54	72	49	94	318
	Hainan	15	9	21	41	71	157
	Shanghai	2	4	3	8	5	22
Nationwide		45,406	48,455	71,268	69,100	70,439	304,668

Abbreviation: PLAD=provincial-level administrative division.

agricultural and livestock farming regions facilitate *Brucella* strain transmission through close human-animal interaction, where livestock farming represents the sole livelihood, complicated by nomadic lifestyles and low socioeconomic conditions.

In southern China, reported cases have increased markedly from 2.0% of national cases in 2019 to 5.38% in 2023, with total cases rising from 4,310 to 10,363. All 15 southern PLADs show upward trends in both case numbers and incidence rates. Molecular epidemiological investigation of *Brucella* in Guizhou from 2009 to 2021 confirms strain importation from northern areas such as Inner Mongolia and Xinjiang (*8*).

The high-risk clusters were predominantly concentrated in the northwestern and northeastern regions, with additional clusters in two southern PLADs, Yunnan and Sichuan. This distribution differs

TABLE 2. Average annual growth rate (%) of incidence (/100,000) in 31 PLADs from 2019 to 2023.

Areas	PLADs	2019–2023, incidence (/100,000)					Average annual incidence (/100,000)	Average annual growth rate (%)
		2019	2020	2021	2022	2023		
Northern	Qinghai	2.45	4.26	13.03	19.51	34.86	14.82	70.02
	Gansu	6.78	11.34	18.39	21.00	22.34	15.97	26.95
	Henan	2.37	3.24	5.06	5.32	5.21	4.24	17.10
	Xinjiang	16.63	12.20	18.68	24.99	36.08	21.71	16.76
	Ningxia	32.59	43.01	70.10	86.83	61.85	58.88	13.67
	Tianjin	0.87	0.87	1.72	1.88	1.53	1.37	11.96
	Shanxi	9.32	9.38	14.21	14.01	14.74	12.33	9.61
	Beijing	0.40	0.25	0.38	0.53	0.60	0.43	8.48
	Liaoning	5.27	6.89	12.87	9.26	7.53	8.37	7.40
	Shaanxi	2.94	2.88	3.59	4.31	3.90	3.53	5.78
	Shandong	2.52	2.41	3.32	3.16	3.26	2.93	5.25
	Hebei	4.51	4.16	6.40	5.33	5.66	5.21	4.63
	Inner Mongolia	55.83	64.60	91.11	79.53	68.34	71.88	4.12
	Jilin	4.40	4.28	5.45	3.57	4.66	4.47	1.12
	Heilongjiang	11.47	7.88	12.93	9.12	10.93	10.46	−0.95
	Xizang	1.60	1.65	1.34	0.55	0.60	1.15	−17.69
Southern	Guizhou	0.09	0.15	0.24	0.36	0.54	0.28	42.39
	Yunnan	0.66	0.79	1.48	2.22	3.24	1.68	37.25
	Hainan	0.16	0.10	0.21	0.40	0.69	0.31	33.93
	Sichuan	0.14	0.16	0.25	0.32	0.50	0.27	29.51
	Hubei	0.14	0.12	0.19	0.30	0.43	0.24	26.31
	Jiangxi	0.12	0.11	0.23	0.18	0.39	0.21	25.65
	Anhui	0.22	0.36	0.58	0.57	0.68	0.48	24.64
	Shanghai	0.01	0.02	0.01	0.03	0.02	0.02	19.47
	Guangxi	0.31	0.25	0.46	0.49	0.73	0.45	18.54
	Jiangsu	0.18	0.20	0.34	0.33	0.35	0.28	14.76
	Chongqing	0.16	0.17	0.22	0.15	0.29	0.20	13.11
	Hunan	0.31	0.24	0.36	0.37	0.53	0.36	11.45
	Zhejiang	0.19	0.22	0.28	0.32	0.30	0.26	9.51
	Fujian	0.38	0.28	0.47	0.49	0.57	0.44	8.20
	Guangdong	0.40	0.31	0.38	0.39	0.48	0.39	3.77
Nationwide		3.25	3.45	5.06	4.90	5.00	4.33	8.97

Abbreviation: PLAD=provincial-level administrative division.

from the 2004–2019 pattern, where significant spatial correlations of high incidence were primarily confined to northern China, particularly Inner Mongolia, Shanxi, and Heilongjiang (*9*). In Jiangsu, the disease progression from 2006 to 2021 showed gradual expansion from northern and southern regions toward central areas. This situation necessitates urgent enhancement of local outbreak response capabilities in high-incidence regions.

The control of human brucellosis is fundamentally dependent on effective animal brucellosis surveillance and control measures. However, the ongoing development of animal husbandry presents significant challenges to animal brucellosis prevention and control (*10*). Strict enforcement of regulations prohibiting the movement of infected animals from northern to southern areas is crucial, including systematic screening and isolation of diseased animals from herds, and

TABLE 3. Joinpoint regression analysis of human brucellosis in 31 PLADs from 2019 to 2023.

Areas	PLADs	Period	APC	95% *CI*	*P*
Northern	Qinghai	2019–2023	97.97	69.82, 129.00	<0.001
	Gansu	2019–2023	35.02	−0.79, 82.97	0.063
	Xinjiang	2019–2023	25.44	−1.55, 58.41	0.070
	Henan	2019–2023	23.05	1.99, 47.46	0.024
	Ningxia	2019–2023	21.95	−20.49, 86.16	0.320
	Tianjin	2019–2023	20.91	−14.88, 71.26	0.266
	Beijing	2019–2023	16.81	−6.27, 44.65	0.188
	Shanxi	2019–2023	14.09	1.60, 27.52	0.020
	Liaoning	2019–2023	10.62	−19.40, 49.80	0.472
	Shaanxi	2019–2023	10.14	−5.45, 27.97	0.206
	Shandong	2019–2023	8.16	−0.29, 16.88	0.061
	Hebei	2019–2023	7.26	−3.07, 18.19	0.180
	Inner Mongolia	2019–2023	6.31	−9.43, 24.12	0.419
	Heilongjiang	2019–2023	0.50	−24.41, 32.65	0.971
	Jilin	2019–2023	−0.70	−14.26, 14.34	0.891
	Xizang	2019–2023	−26.32	−45.07, −1.92	0.035
Southern	Guizhou	2019–2023	55.67	48.68, 62.84	<0.001
	Hainan	2019–2023	54.66	9.50, 115.38	0.008
	Yunnan	2019–2023	52.19	41.92, 62.91	<0.001
	Sichuan	2019–2023	39.18	23.83, 56.00	<0.001
	Hubei	2019–2023	38.07	6.19, 78.88	0.011
	Jiangxi	2019–2023	31.36	8.88, 57.77	<0.001
	Anhui	2019–2023	30.46	9.96, 53.80	0.001
	Shanghai	2019–2023	27.69	−3.12, 66.00	0.080
	Guangxi	2019–2023	26.76	10.13, 45.20	<0.001
	Jiangsu	2019–2023	20.53	6.08, 36.22	0.003
	Hunan	2019–2023	16.45	−2.44, 38.56	0.103
	Fujian	2019–2023	14.56	−0.73, 31.89	0.068
	Zhejiang	2019–2023	13.82	−1.66, 31.38	0.088
	Chongqing	2019–2023	11.71	−9.84, 37.80	0.334
	Guangdong	2019–2023	5.96	−15.45, 32.30	0.499
Nationwide		2019–2023	12.86	1.33, 25.09	0.028

Abbreviation: PLAD=provincial-level administrative division; *CI*=confidence interval; APC=annual percent change.

continued vaccination programs. Remarkably, resource and financial investment in brucellosis control must be continuously increased to curb its spread, even after achieving initial control (*11*).

This study has several limitations. Brucellosis is frequently underreported due to its nonspecific clinical presentation, and our analysis relies on surveillance system data that may be influenced by regional variations in physician awareness of the disease.

Our analysis demonstrates that the disease has not only persisted in northern China but has also established significant presence in southern PLADs. The proportion of total reported cases in southern regions has increased markedly from 2.0% before 2019 to 5.38% after 2019. These findings underscore the urgent need to implement more stringent control strategies to prevent further deterioration of the situation.

Conflicts of interest: No conflicts of interest.

Acknowledgements: We acknowledge the

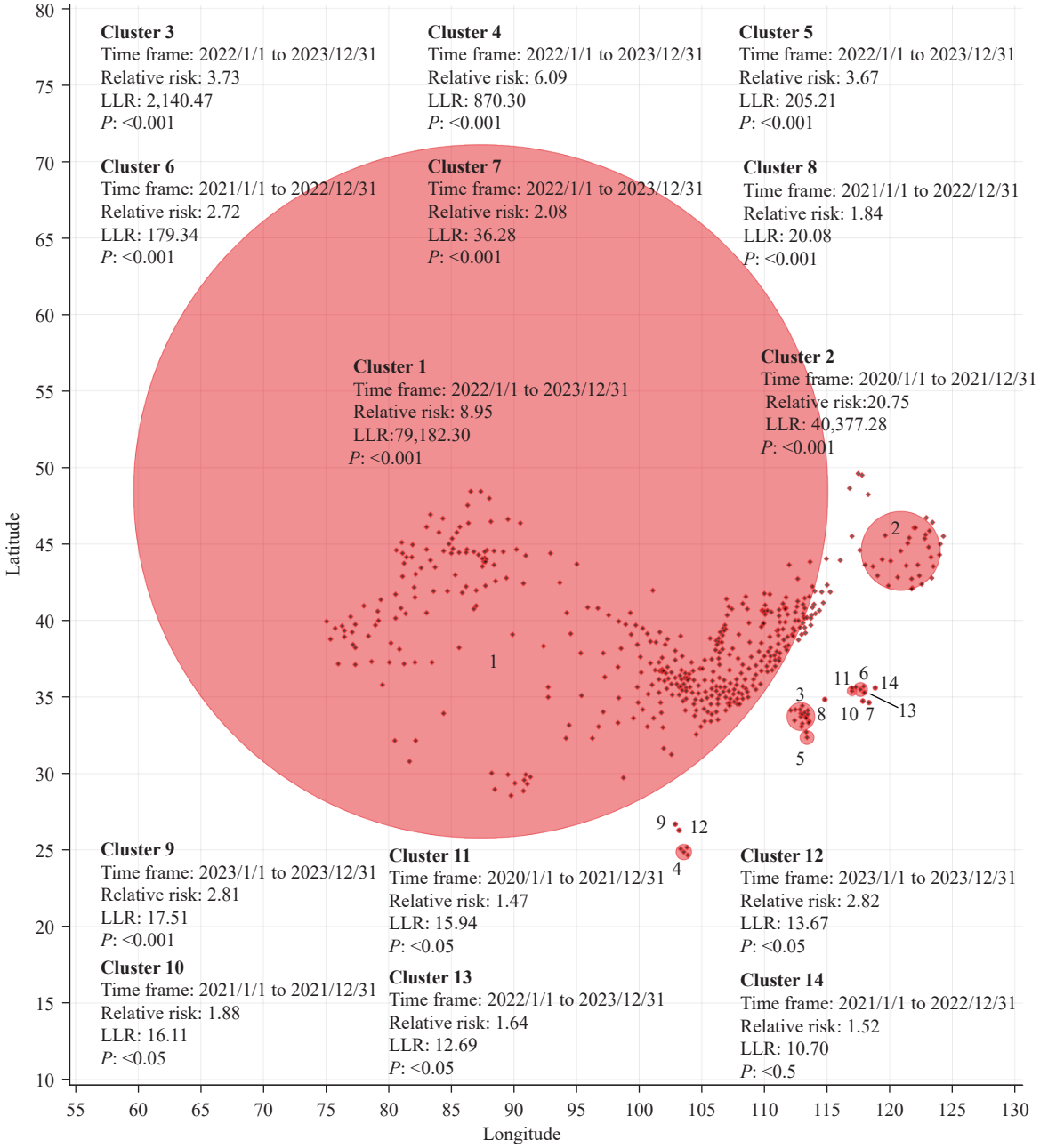

FIGURE 2. Spatial-temporal feature of human brucellosis in China, from 2019 to 2023.
Note: Retrospective space-time analysis scanning for clusters with high rates using the Discrete Poisson model; numbers (1–14) in figures indicates location of 14 clusters zones.
Abbreviation: LLR=log likelihood ratio.

dedication of healthcare staff at provincial, prefecture, and county-level CDCs across the 31 PLADs and XPCC in China for their contributions to brucellosis surveillance and control efforts.

Funding: Supported by the National Natural Science Foundation of China (No. L2124006, Institute Number: 90100). The funding body had no role in study design, data collection and analysis, decision to publish, or manuscript preparation.

doi: 10.46234/ccdcw2025.020

[#] Corresponding authors: Zhenjun Li, lizhenjun@icdc.cn; Canjun Zheng, zhengcj@chinacdc.cn.

[1] National Key Laboratory of Intelligent Tracking and Forecasting for Infectious Diseases, National Institute for Communicable Disease Control and Prevention, Chinese Center for Disease Control and Prevention, Beijing, China; [2] Chinese Center for Disease Control and Prevention, Beijing, China; [3] National Institute of Parasitic Diseases,

TABLE 4. Distribution profile of high-high clusters of human brucellosis from 2019 to 2023.

Clusters	Time frame	Relative risk	LLR	Number of counties	PLADs
1	2022/1/1 to 2023/12/31	8.95	79182.30	419	Xinjiang, Inner Mongolia, Gansu, Qinghai, Ningxia, Xizang, Sichuan, Shanxi, Shaanxi, Hebei
2	2020/1/1 to 2021/12/31	20.75	40377.28	33	Inner Mongolia, Jilin, Liaoning, Heilongjiang
3	2022/1/1 to 2023/12/31	3.73	2140.47	19	Henan
4	2022/1/1 to 2023/12/31	6.09	870.29	4	Yunnan
5	2022/1/1 to 2023/12/31	3.67	205.21	2	Henan
6	2021/1/1 to 2022/12/31	2.72	179.34	3	Shandong
7	2022/1/1 to 2023/12/31	2.08	36.28	1	Shandong
8	2021/1/1 to 2022/12/31	1.84	20.08	1	Henan
9	2023/1/1 to 2023/12/31	2.81	17.51	1	Sichuan
10	2021/1/1 to 2021/12/31	1.88	16.11	1	Shandong
11	2020/1/1 to 2021/12/31	1.47	15.94	2	Shandong
12	2023/1/1 to 2023/12/31	2.82	13.67	1	Yunnan
13	2022/1/1 to 2023/12/31	1.64	12.69	1	Shandong
14	2021/1/1 to 2022/12/31	1.52	10.70	1	Shandong

Note: Number of counties: total of counties involved in the high-risk clusters zone.
Abbreviation: LLR=log likelihood ratio; PLAD=provincial-level administrative division.

Chinese Center for Disease Control and Prevention (Chinese Center for Tropical Diseases Research), Shanghai, China.
[&] Joint first authors.

Submitted: September 13, 2024
Accepted: December 03, 2024
Issued: January 24, 2025

REFERENCES

1. Xu QG. Knowledge, attitude and practice associated with brucellosis in occupational risk groups in China [dissertation]. Bangkok, Thailand: Chulalongkorn University; 2021. https://digital.car.chula.ac.th/chulaetd/4950/.
2. Dutkiewicz J, Cisak E, Sroka J, Wójcik-Fatla A, Zając V. Biological agents as occupational hazards-selected issues. Ann Agric Environ Med 2011;18(2):286-93. https://www.aaem.pl/Biological-agents-as-occupational-hazards-selected-issues,71702,0,2.html.
3. Lai SJ, Zhou H, Xiong WY, Yu HJ, Huang ZJ, Yu JX, et al. Changing epidemiology of human brucellosis, China, 1955-2014. Emerg Infect Dis 2017;23(2):184 – 94. https://doi.org/10.3201/eid2302.151710.
4. Yang HM, Chen QL, Li Y, Mu D, Zhang YP, Yin WW. Epidemic characteristics, high-risk areas and space-time clusters of human brucellosis — China, 2020–2021. China CDC Wkly 2023;5(1):17 – 22. https://doi.org/10.46234/ccdcw2023.004.
5. Tao ZF, Chen QL, Chen YS, Li Y, Mu D, Yang HM, et al. Epidemiological characteristics of human brucellosis - China, 2016-2019. China CDC Wkly 2021;3(6):114 – 9. https://doi.org/10.46234/ccdcw2021.030.
6. Kim HJ, Fay MP, Feuer EJ, Midthune DN. Permutation tests for joinpoint regression with applications to cancer rates. Stat Med 2000;19(3):335 – 51. https://doi.org/10.1002/(sici)1097-0258(20000215)19:3<335::aid-sim336>3.0.co;2-z.
7. Zhou LH, Fan M, Hou Q, Jin Z, Sun XD. Transmission dynamics and optimal control of brucellosis in Inner Mongolia of China. Math Biosci Eng 2018;15(2):543 – 67. https://doi.org/10.3934/mbe.2018025.
8. Tan QQ, Wang Y, Liu Y, Tao ZF, Yu C, Huang Y, et al. Molecular epidemiological characteristics of *Brucella* in Guizhou Province, China, from 2009 to 2021. Front Microbiol 2023;14:1188469. https://doi.org/10.3389/fmicb.2023.1188469.
9. Sun ZX, Wang Y, Li YJ, Yu SH, Wu W, Huang DS, et al. Socioeconomic, meteorological factors and spatiotemporal distribution of human brucellosis in China between 2004 and 2019-a study based on spatial panel model. PLoS Negl Trop Dis 2023;17(11):e0011765. https://doi.org/10.1371/journal.pntd.0011765.
10. Qureshi KA, Parvez A, Fahmy NA, Abdel Hady BH, Kumar S, Ganguly A, et al. Brucellosis: epidemiology, pathogenesis, diagnosis and treatment-a comprehensive review. Ann Med 2023;55(2):2295398. https://doi.org/10.1080/07853890.2023.2295398.
11. El-Sayed A, Awad W. Brucellosis: evolution and expected comeback. Int J Vet Sci Med 2018;6(Suppl):S31 – 5. https://doi.org/10.1016/j.ijvsm.2018.01.008.

Preplanned Studies

Multicenter Study on the Prevalence of Human Respiratory Syncytial Virus Coinfection and Disease Burden Among Hospitalized Children Aged 5 Years and Younger — 5 Prefecture-level Cities, Zhejiang Province, China, 2018–2023

Wanwan Sun[1,&]; An Zhu[2,&]; Zhiyong Zhu[3,&]; Jinren Pan[1]; Chaorong Ni[4]; Wenjie Wu[5]; An Tang[5]; Lei Guo[6]; Zhao Yu[1]; Xicheng Gu[7]; Yu Zhang[8]; Xiaofei Fu[9,#]; Yongqiang Shao[10,#]; Shelan Liu[1,#]

Summary

What is already known about this topic?

Human respiratory syncytial virus (HRSV) coinfection with other respiratory pathogens frequently occurs in young children with acute respiratory illness. However, the epidemiological patterns and associated disease burden of HRSV coinfections in pediatric populations remain poorly characterized.

What is added by this report?

Analysis of hospitalized children under 5 years in Zhejiang Province from 2018 to 2023 revealed that 20.4% experienced HRSV coinfections, with bacterial coinfections substantially exceeding viral coinfections (14.1% *vs.* 5.3%). *M. pneumoniae* and *S. pneumoniae* emerged as predominant bacterial copathogens, while human rhinovirus and cytomegalovirus were the most prevalent viral coinfection agents. HRSV coinfections were associated with significantly higher disease burden compared to HRSV monoinfection [median expense: 4,971.4 Chinese Yuan (CNY) *vs.* 4,649.1 CNY; $P<0.05$].

What are the implications for public health practice?

Implementation of comprehensive prevention strategies, including vaccination programs, nonpharmaceutical interventions, and enhanced surveillance of multiple respiratory pathogens, is essential to reduce HRSV coinfections and their associated disease burden during periods of high respiratory pathogen circulation.

The human respiratory syncytial virus (HRSV) belongs to the *Orthopenumovirus* genus within the *Pneumoviridae* family (*1*) and represents the primary etiological agent of acute lower respiratory tract infections (ALRTIs) in children under 5 years, immunocompromised individuals, and elderly populations (*2*–*3*). Globally in 2019, HRSV was responsible for 33 million ALRTI episodes, resulting in 3.6 million hospitalizations and 101,400 deaths among children younger than 5 years (*1*). China bears a substantial burden of HRSV infections, accounting for more than 10% of global cases (*4*).

Advanced diagnostic technologies in hospital settings have revealed an increasing frequency of HRSV codetection with other respiratory viruses (*5*). Contemporary research indicates that HRSV codetection with other respiratory viruses occurs in 35%–40% of HRSV infections among young children (*6*–*7*). However, the impact of viral and bacterial coinfections on the disease burden of HRSV-associated respiratory illnesses remains incompletely understood (*8*).

This study examined hospitalized children aged ≤5 years admitted with influenza-like illness (ILI), acute respiratory infection (ARI), or severe acute respiratory infection (SARI) (Supplementary File 1, available at https://weekly.chinacdc.cn/) between January 1, 2018, and August 31, 2023, across eight hospitals in Zhejiang Province. HRSV infection was confirmed through laboratory antigen testing or reverse transcription polymerase chain reaction (RT-PCR). Hospital selection criteria incorporated geographical location, economic development level, and population coverage considerations (Supplementary File 2 Supplementary Table S1, available at https://weekly.chinacdc.cn/). Total hospitalization costs encompassed all direct patient expenses during admission, including examination, medication, bed, and treatment fees. To account for temporal cost variations across the 5-year study period, this research applied a 3% discount rate (*9*) to adjust hospitalization costs from 2018–2022.

This study stratified patients into four categories

based on pathogen infection status: HRSV alone, HRSV+virus, HRSV+bacteria, and HRSV+virus+bacteria. Pathogen positivity rates were compared across these groups, considering gender, age group, pneumonia status, coronavirus disease 2019 (COVID-19) epidemic phases, and hospitalization duration. This study analyzed the pathogen spectrum in HRSV coinfection cases and evaluated the hospitalization duration and total costs associated with the three most prevalent viral and bacterial coinfections.

Statistical analyses were conducted using R software version 4.3.1 (R Foundation for Statistical Computing, Vienna, Austria). Statistical significance was established at $P<0.05$ (two-tailed).

Between January 2018 and August 2023, the eight participating hospitals recorded 8,338,484 outpatient and 252,658 inpatient visits across all age groups. Of these, 180,601 patients underwent HRSV testing via nucleic acid or antigen detection methods, yielding 10,956 positive cases (positivity rate: 6.07%). The highest monthly positivity rates were observed in August 2021 (26.9%) and December 2018 (25.9%), while no positive cases were detected in May and June 2020 (Figure 1A).

Among the 7,857 HRSV-positive inpatients aged 5 years and younger included in this study, the median age was 12.0 months [interquartile range (IQR): 4.0–24.0 months], with 65.9% being 12.0 months or younger. Males comprised 60.4% (4,746/7,857) of the cohort, and 80.9% (6,360/7,857) were diagnosed with

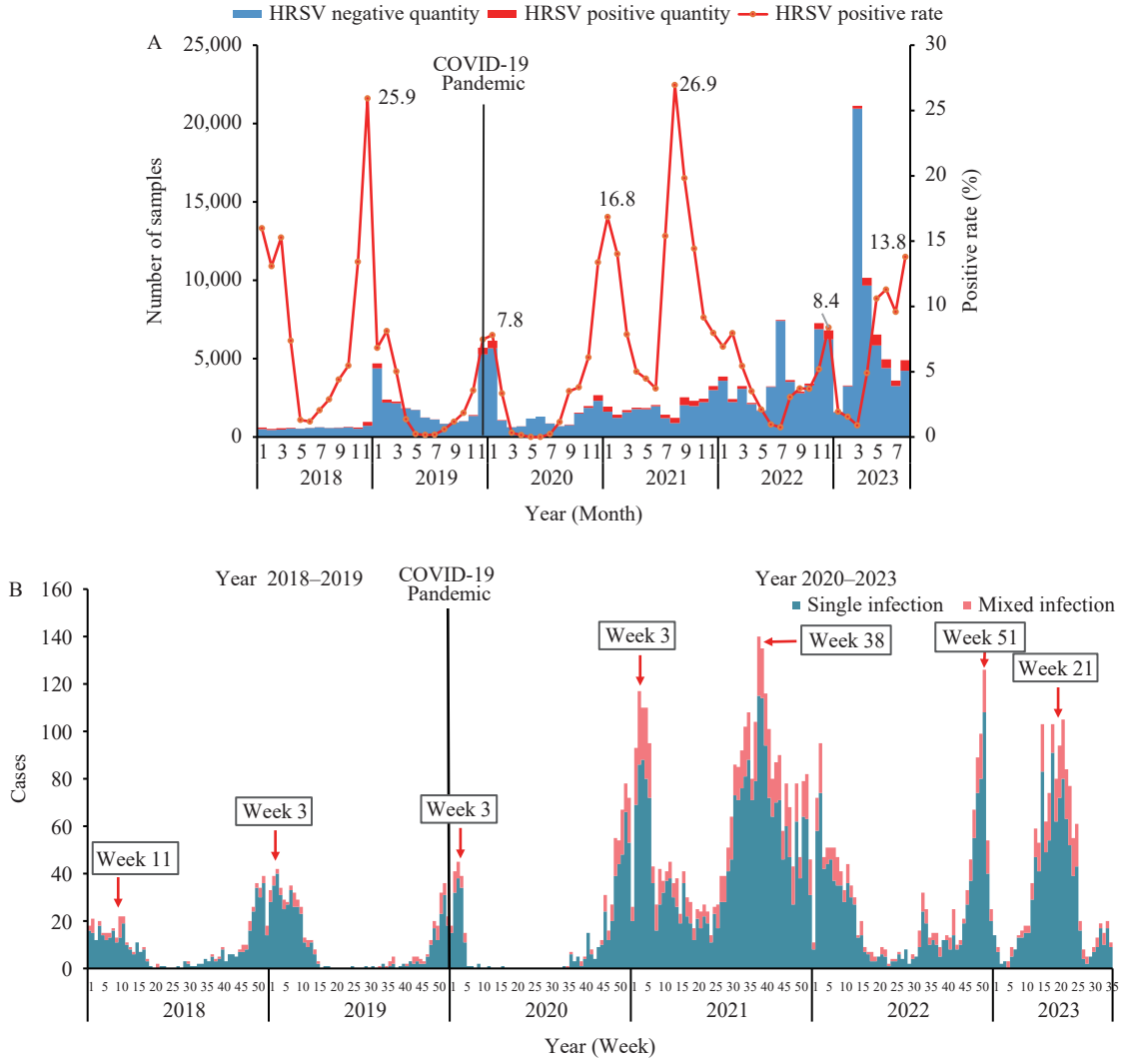

FIGURE 1. The timeline distribution of HRSV monoinfections and coinfections among outpatients and inpatients in Zhejiang Province, China, 2018–2023. (A) Monthly detection rates of HRSV among outpatients and inpatients; (B) Weekly distribution of HRSV monoinfections and coinfections among hospitalized children aged 5 years and younger.
Abbreviation: COVID-19=coronavirus disease 2019; HRSV=human respiratory syncytial virus.

pneumonia. HRSV coinfection with other pathogens was identified in 20.4% (1,601/7,857) of cases.

A significant increase in HRSV hospitalizations was observed from 2020 to 2023 compared to 2018–2019 (Figure 1A). The median age of patients during the COVID-19 pandemic period (2020–2023) was significantly higher than in the pre-pandemic period (2018–2019) (17.0 months *vs*. 10.1 months, *P*<0.010). The pandemic period saw a reduction in the proportion of HRSV inpatients aged 0–5 months (from 45% to 28%) and concurrent increases in those aged 13–24 months (from 9% to 15%) and 25–36 months (from 6% to 15%) (Supplementary Figure S1, available at https://weekly.chinacdc.cn/).

Compared to HRSV mono-infection cases, patients with coinfections were significantly older (19.7 months *vs*. 15.0 months, *P*<0.01) (Table 1). Notable increases were observed in the 13-24 months (13% to 18%) and 25-36 months (12% to 20%) age groups (Supplementary Figure S2, available at https://weekly.chinacdc.cn/). Coinfection rates were lower in males compared to females (18.8% *vs*. 22.7%, *P*<0.01) and higher in pneumonia cases compared to non-pneumonia cases (21.9% *vs*. 14.1%, *P*<0.01), Table 1. The highest coinfection rates were observed in patients with hospital stays of 15 days (31.2%), followed by those staying 8–14 days (21.7%) (Table 1).

Among the HRSV inpatients, 14.1% (1,110/7,857) tested positive for at least one bacterial pathogen. Patients with bacterial coinfections demonstrated a substantially higher incidence of pneumonia compared to those with viral coinfections (73.2% *vs*. 22.7%).

TABLE 1. Pathogen positivity rates among hospitalized children aged ≤5 years with human respiratory syncytial virus infections in multicenter surveillance, Zhejiang Province, China.

Categories	Number (*N*=7,857)	Mono-HRSV infection (n1=6,256)	Co-HRSV infection				*P*
			Total (n2=1,601)	HRSV+virus (n3=418)	HRSV+bacteria (n4=1,110)	HRSV+virus+bactetia (n5=73)	
Proportion, No. (%)	7,857 (100.0)	6,256 (79.6)	1,601 (20.4)	418 (26.1)	1,110 (69.3)	73 (4.6)	–
Gender, No. (%)							
Male	4,746 (60.4)	3,852 (81.2)	894 (18.8)	256 (28.6)	599 (67.0)	39 (4.4)	<0.0001
Female	3,111 (39.6)	2,404 (77.3)	707 (22.7)	162 (22.9)	511 (72.3)	34 (4.8)	
Mean age (months)	15.9	15.0	19.7	16.4	20.9	20.9	
Age group (months), No. (%)							
0–5	2,383 (30.3)	2,085 (87.5)	298 (12.5)	135 (45.3)	150 (50.3)	13 (4.4)	0.035
6–12	2,816 (35.8)	2,225 (79.0)	591 (21.0)	147 (24.9)	421 (71.2)	23 (3.9)	0.663
13–24	1,124 (14.3)	841 (74.8)	283 (25.2)	60 (21.2)	207 (73.1)	16 (5.7)	0.004
25–36	1,039 (13.2)	735 (70.7)	304 (29.3)	56 (18.4)	234 (77.0)	14 (4.6)	0
37–48	376 (4.8)	274 (72.9)	102 (27.1)	14 (13.7)	82 (80.4)	6 (5.9)	0.007
49–60	119 (1.6)	96 (80.7)	23 (19.3)	6 (26.1)	16 (69.6)	1 (4.3)	Reference group
Pneumonia or not, No. (%)							
Yes	6,360 (81.0)	4,970 (78.1)	1,390 (21.9)	315 (22.7)	1,017 (73.2)	58 (4.1)	0
No	1,497 (19.0)	1,286 (85.9)	211 (14.1)	103 (48.8)	93 (44.1)	15 (7.1)	
Period, No. (%)							
Year 2018–2019	1,081 (13.8)	925 (85.6)	156 (14.4)	53 (34.0)	99 (63.5)	4 (2.5)	0
Year 2020–2023	6,776 (86.2)	5,331 (78.7)	1,445 (21.3)	365 (25.3)	1,011 (70.0)	69 (4.7)	
Hospitalization duration (day)							
1–3	950 (12.1)	827 (87.1)	123 (12.9)	43 (35.0)	78 (63.4)	2 (1.6)	0
4–7	5,847 (74.4)	4,605 (78.7)	1,242 (21.2)	290 (23.3)	898 (72.3)	54 (4.4)	0.052
8–14	996 (12.7)	780 (78.3)	216 (21.7)	73 (33.8)	129 (59.7)	14 (6.5)	0.075
>15	64 (0.8)	44 (68.8)	20 (31.2)	12 (60.0)	5 (25.0)	3 (15.0)	Reference group

Note: *P* comparing mono-HRSV infection *vs*. co-HRSV infection.
Abbreviation: HRSV=human respiratory syncytial virus.

Additionally, the rate of bacterial coinfections was significantly elevated during the 2020–2023 period compared to 2018–2019 (Table 1).

In bacterial coinfection cases, *Mycoplasma pneumoniae* (*M. pneumoniae*) emerged as the predominant pathogen, representing 59.2% of all bacterial detections. This was followed by *Streptococcus pneumoniae* (*S. pneumoniae*) at 25.3% and *Haemophilus influenzae* (*H. influenzae*) at 8.8% (Figure 2).

Among viral coinfections, human rhinovirus (HRV) was the most frequently detected pathogen, accounting for 27.3% of all viral-positive detections, followed by cytomegalovirus (CMV; 23.8%) and human adenovirus (HAdV; 14.0%) (Figure 2).

Analysis of hospitalization expenses revealed that HRSV coinfection cases, whether viral or bacterial, incurred significantly higher costs (median: 4,971.4, IQR: 3,864.7–6,878.0) compared to HRSV monoinfection cases (median: 4,649.1, IQR: 3,486.6–6,524.9, P=0.013). Among all coinfections, CMV was associated with the highest median

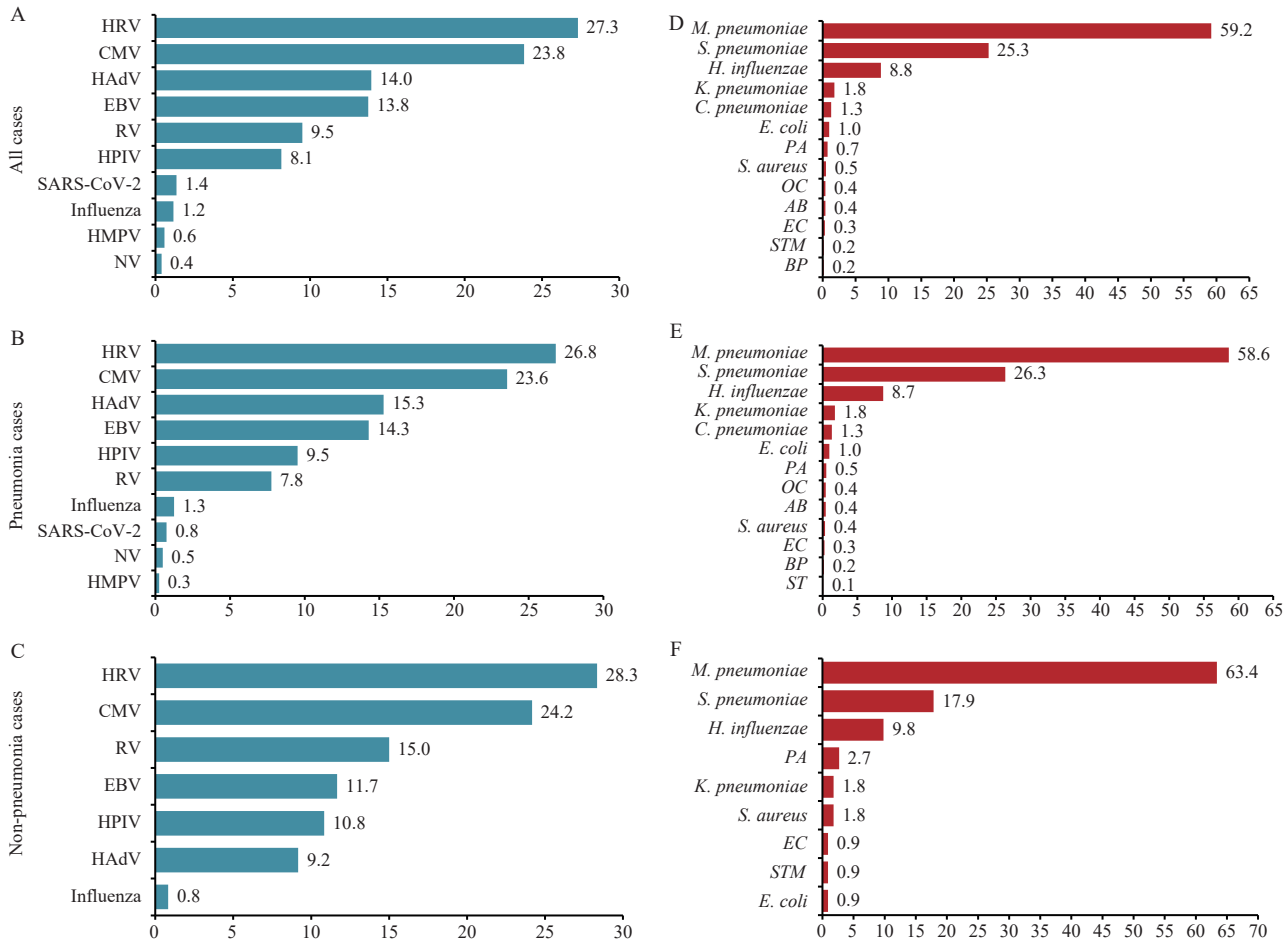

FIGURE 2. Viral and bacterial composition of HRSV-positive hospitalized children aged 5 years and younger in Zhejiang Province, China, 2018–2023. (A) Viral composition in all patients; (B) Viral composition in pneumonia cases; (C) Viral composition in non-pneumonia cases; (D) Bacterial composition in all cases; (E) Bacterial composition in pneumonia cases; (F) Bacterial composition in non-pneumonia cases.

Note: Analysis includes all cases tested for ten viral and 13 bacterial pathogens among HRSV-positive hospitalized children. Bar lengths and accompanying numbers represent the proportion of each pathogen, calculated as the number of positive cases divided by the total number of HRSV-positive cases.

Abbreviation: HRV=human rhinovirus; CMV=cytomegalovirus; HAdV=human adenovirus; EBV=Epstein-Barr virus; RV=rotavirus; HPIV=human parainfluenza virus; COVID-19=coronavirus disease 2019; HMPV=human metapneumovirus; NV=norovirus; *M. pneumoniae=Mycoplasma pneumoniae*; *S. pneumoniae=Streptococcus pneumoniae*; *H. influenzae=Haemophilus influenzae*; *K. pneumoniae=Klebsiella pneumoniae*; *C. pneumoniae=Chlamydia pneumoniae*; *E. coli=Escherichia coli*; *PA=Pseudomonas aeruginosa*; *S. aureus=Staphylococcus aureus*; *OC=oral candidiasis*; *AB=Acinetobacter baumannii*; *EC=Enterobacter cloacae*; *BP=Bordetella pertussis*; *ST=Salmonella typhi*; *STM=Salmonella typhimurium*.

hospitalization expense (median: 7,243.6, IQR: 5,459.3–9,569.8) (Figure 3).

Regarding length of stay, cases with viral or bacterial coinfections demonstrated marginally longer durations (median: 5.0, IQR: 4.0–7.0) compared to HRSV monoinfections (median: 5.0, IQR: 4.0–6.0, *P*<0.01). Among viral coinfections, CMV cases exhibited significantly extended hospitalization periods (median: 6.0, IQR: 5.0–8.0, *P*=0.003). In bacterial coinfections, both *S. pneumoniae* (median: 6.0, IQR: 5.0–7.0, *P*=0.025) and *H. influenzae* (median: 6.0, IQR: 5.0–7.0, *P*=0.018) demonstrated comparable prolonged hospital stays (Figure 3).

DISCUSSION

This study analyzed surveillance data from 2018 to 2023, encompassing comprehensive pathogen testing data from 8 hospitals in Zhejiang Province for 10 viruses and 13 bacteria in pediatric inpatients under 5 years of age. This analysis revealed significant patterns in the prevalence, pathogen spectrum, and disease burden of HRSV coinfections in this population.

These findings demonstrate a marked increase in HRSV infections during 2020–2023 compared to previous seasons (2018–2019), with a notable shift in age distribution toward older children within the

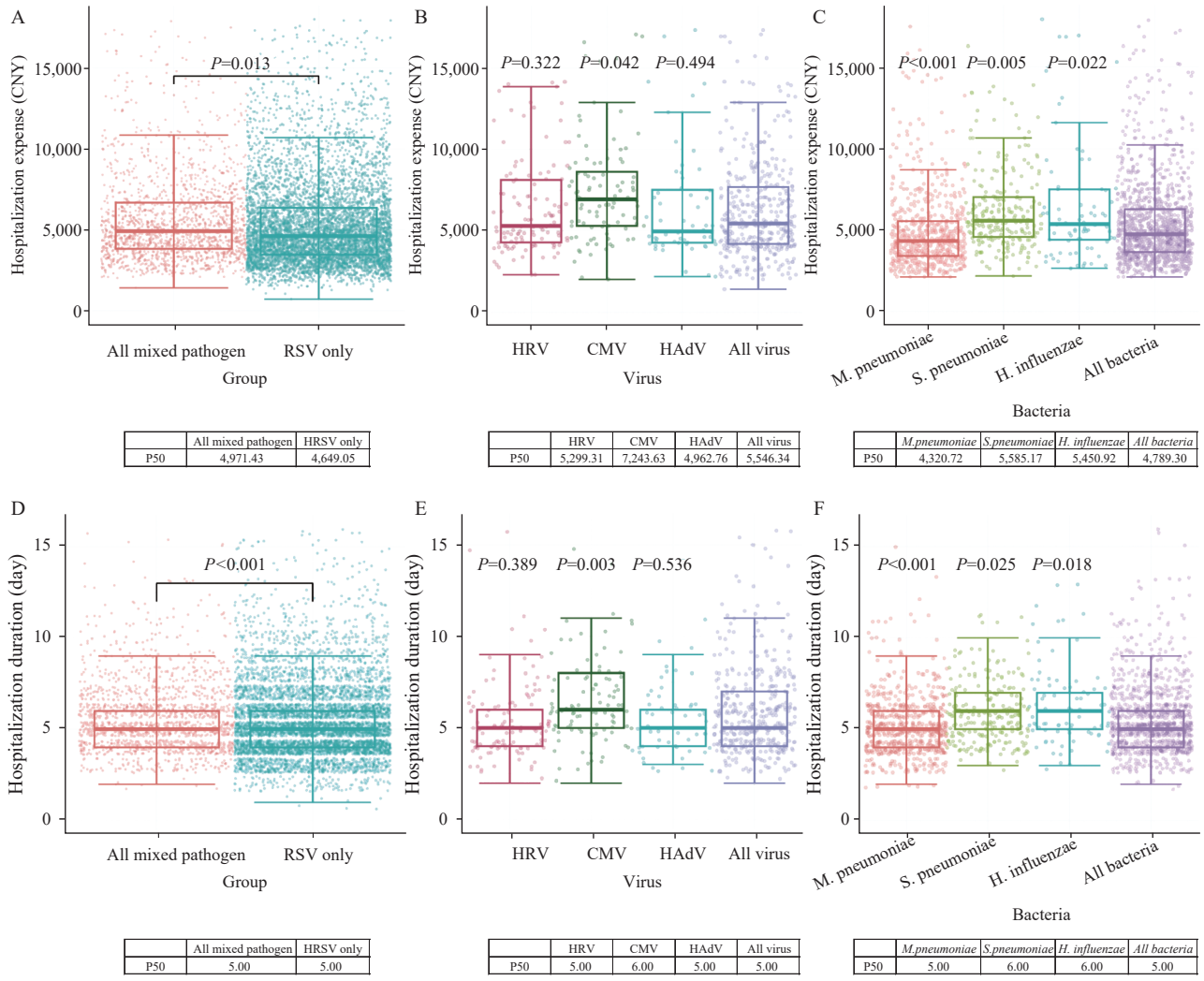

	All mixed pathogen	HRSV only
P50	4,971.43	4,649.05

	HRV	CMV	HAdV	All virus
P50	5,299.31	7,243.63	4,962.76	5,546.34

	M.pneumoniae	*S.pneumoniae*	*H. influenzae*	*All bacteria*
P50	4,320.72	5,585.17	5,450.92	4,789.30

	All mixed pathogen	HRSV only
P50	5.00	5.00

	HRV	CMV	HAdV	All virus
P50	5.00	6.00	5.00	5.00

	M.pneumoniae	*S.pneumoniae*	*H. influenzae*	*All bacteria*
P50	5.00	6.00	6.00	5.00

FIGURE 3. Disease burden in HRSV mono- and co-infections among hospitalized children aged 5 years and younger in Zhejiang Province, China, 2018–2023. (A) Hospitalized expense (HRSV only vs. HRSV coinfection); (B) Hospitalized expense (HRSV coinfections with all viruses vs. single virus); (C) Hospitalized expense (HRSV coinfections with all bacteria vs. single bacteria); (D) Hospitalized days (HRSV only vs. HRSV coinfection); (E) Hospitalized days (HRSV coinfections with all viruses vs. single virus); (F) Hospitalized days (HRSV coinfections with all bacteria vs. single bacteria).
Abbreviation: HRV=human rhinovirus; CMV=cytomegalovirus; HAdV=human adenovirus; *M. pneumoniae=Mycoplasma pneumoniae*; *S. pneumoniae=Streptococcus pneumoniae*; *H. influenzae=Haemophilus influenzae*; CNY=Chinese Yuan.

under-5 age group. This pattern suggests that pandemic-related disruptions created increased susceptibility among older children who lacked prior exposure to endemic HRSV (*9*–*10*).

The study revealed that HRSV coinfection with other respiratory pathogens was common, affecting 20.4% of all hospitalizations during 2018–2023. Notably, HRSV coinfection rates were substantially higher during 2020–2023 compared to 2018–2019. While the precise mechanism remains unclear, this increase likely relates to both enhanced RT-PCR testing implementation and elevated respiratory pathogen circulation during the COVID-19 pandemic period (*11*).

Regarding disease status, HRSV coinfections showed significantly higher prevalence in patients with pneumonia compared to those without pneumonia, aligning with Liu et al.'s findings on coinfection patterns in community-acquired pneumonia (*12*).

This study revealed increased hospital stays and expenses among HRSV coinfections, potentially attributable to the implementation of multiple therapeutic interventions (*13*–*14*). These findings underscore the importance of specialized care for hospitalized children with HRSV coinfections. Optimal management should include isolation in separate wards, with particular emphasis on early detection of coinfections through comprehensive testing for HRSV and other common respiratory viruses, especially in infants under 6 months of age.

This study had two primary limitations. First, the analysis of hospitalization expenses excluded indirect costs. Second, selection bias may have occurred as the study included only inpatients with confirmed HRSV infection, excluding those without HRSV detection.

In conclusion, this study demonstrates a significant increase in HRSV coinfections during the COVID-19 pandemic, particularly among patients with pneumonia and those requiring extended hospitalization exceeding 14 days. These coinfections were associated with prolonged hospital stays and elevated healthcare costs. To mitigate future HRSV coinfection incidence and disease burden, public health initiatives should focus on raising awareness among parents and the general public regarding pediatric coinfection risks and prevention strategies. Healthcare providers should implement recommended testing protocols for patients presenting with acute respiratory symptoms to identify HRSV coinfections promptly, potentially reducing infection severity and associated disease burden.

Conflicts of interest: No conflicts of interest.

Acknowledgments: The contributions of the local hospitals and prefecture Centers for Disease Control and Prevention in China for their assistance with data collection and field investigations.

Funding: Supported by the Zhejiang Provincial Program for the Cultivation of High-Level Innovative Health Talents and Zhejiang Provincial Disease Control and Prevention Administration (2025JK008), as well as the Key Program of Health Commission of Zhejiang Province/Science Foundation of National Health Commission (WKJ-ZJ-2523) and the Key Projects of the National Natural Science Foundation of China (U23A20496).

doi: 10.46234/ccdcw2025.021

[#] Corresponding authors: Shelan Liu, slliu@cdc.zj.cn; Yongqiang Shao, wzsyq@126.com; Xiaofei Fu, cfk@jxcdc.org.cn.

[1] Department of Infectious Diseases, Zhejiang Provincial Center for Disease Control and Prevention, Hangzhou City, Zhejiang Province, China; [2] Department of Pediatrics, Second People's Hospital of Jinyun County (Huzhen Branch of Lishui Central Hospital), Lishui City, Zhejiang Province, China; [3] Department of Infectious Diseases, Tonglu County Center for Disease Control and Prevention (Tonglu County Health Supervision Institute), Hangzhou City, Zhejiang Province, China; [4] Department of Infectious Diseases, Wenzhou Center for Disease Control and Prevention (Wenzhou Health Supervision Institution), Wenzhou City, Zhejiang Province, China; [5] Department of Infectious Diseases, Zhoushan Center for Disease Control and Prevention, Zhoushan City, Zhejiang Province, China; [6] Department of Infection Control, Second Affiliated Hospital and Yuying Children's Hospital of Wenzhou Medical University, Wenzhou City, Zhejiang Province, China; [7] University of Rochester, Rochester, New York, USA; [8] Tonglu Hospital of the First People's Hospital of Hangzhou, Hangzhou City, Zhejiang Province, China; [9] Department of Infectious Disease Control and Prevention, Jiaxing Center for Disease Control and Prevention, Jiaxing City, Zhejiang Province, China; [10] Wenzhou Central Hospital, Wenzhou City, Zhejiang Province, China.
[&] Joint first authors.

Submitted: September 27, 2024
Accepted: December 29, 2024
Issued: January 24, 2025

REFERENCES

1. Wang X, Li Y, Shi T, Bont LJ, Chu HY, Zar HJ, et al. Global disease burden of and risk factors for acute lower respiratory infections caused by respiratory syncytial virus in preterm infants and young children in 2019: a systematic review and meta-analysis of aggregated and individual participant data. Lancet 2024;403(10433):1241 – 53. https://doi.org/10.1016/S0140-6736(24)00138-7.
2. Rima B, Collins P, Easton A, Fouchier R, Kurath G, Lamb RA, et al. ICTV virus taxonomy profile: *Pneumoviridae*. J Gen Virol 2017;98(12): 2912 – 3. https://doi.org/10.1099/jgv.0.000959.
3. Obando-Pacheco P, Justicia-Grande AJ, Rivero-Calle I, Rodríguez-Tenreiro C, Sly P, Ramilo O, et al. Respiratory syncytial virus

seasonality: a global overview. J Infect Dis 2018;217(9):1356 – 64. https://doi.org/10.1093/infdis/jiy056.
4. Chinese Center for Disease Control and Prevention. Q&A on HRSV. 2023. https://en.chinacdc.cn/in_focus/202302/t20230215_263733.html. [2023-2-15].
5. Li Y, Pillai P, Miyake F, Nair H. The role of viral co-infections in the severity of acute respiratory infections among children infected with respiratory syncytial virus (RSV): a systematic review and meta-analysis. J Glob Health 2020;10(1):010426. https://doi.org/10.7189/jogh.10.010426.
6. Lee JT, Chang LY, Wang LC, Kao CL, Shao PL, Lu CY, et al. Epidemiology of respiratory syncytial virus infection in northern Taiwan, 2001-2005--seasonality, clinical characteristics, and disease burden. J Microbiol Immunol Infect 2007;40(4):293-301. https://pubmed.ncbi.nlm.nih.gov/17712463/.
7. Yoon JG, Noh JY, Choi WS, Park JJ, Suh YB, Song JY, et al. Clinical characteristics and disease burden of respiratory syncytial virus infection among hospitalized adults. Sci Rep 2020;10(1):12106. https://doi.org/10.1038/s41598-020-69017-8.
8. Bourzac K. Respiratory syncytial virus co-infections might conspire to worsen disease. Nature 2023;621(7980):S60 – 1. https://doi.org/10.1038/d41586-023-02959-x.
9. Suss RJ, Simões EAF. Respiratory syncytial virus hospital-based burden of disease in children younger than 5 years, 2015-2022. JAMA Netw Open 2024;7(4):e247125. https://doi.org/10.1001/jamanetworkopen.2024.7125.
10. Hamid S, Winn A, Parikh R, Jones JM, McMorrow M, Prill MM, et al. Seasonality of respiratory syncytial virus - United States, 2017-2023. MMWR Morb Mortal Wkly Rep 2023;72(14):355 – 61. https://doi.org/10.15585/mmwr.mm7214a1.
11. Pan ZY, Wang W, Zhang C, Mao LW, Li YR, Yuan LL, et al. A rapid, sensitive, and high-throughput pathogen detection method and application of identifying pathogens based on multiplex PCR technology combined with capillary electrophoresis. Diagn Microbiol Infect Dis 2025;111(1):116563. https://doi.org/10.1016/j.diagmicrobio.2024.116563.
12. Liu YN, Zhang YF, Xu Q, Qiu Y, Lu QB, Wang T, et al. Infection and co-infection patterns of community-acquired pneumonia in patients of different ages in China from 2009 to 2020: a national surveillance study. Lancet Microbe 2023;4(5):e330 – 9. https://doi.org/10.1016/S2666-5247(23)00031-9.
13. Bakaletz LO. Viral-bacterial co-infections in the respiratory tract. Curr Opin Microbiol 2017;35:30 – 5. https://doi.org/10.1016/j.mib.2016.11.003.
14. Adams K, Tastad KJ, Huang S, Ujamaa D, Kniss K, Cummings C, et al. Prevalence of SARS-CoV-2 and influenza coinfection and clinical characteristics among children and adolescents aged <18 years who were hospitalized or died with influenza – United States, 2021-22 influenza season. MMWR Morb Mortal Wkly Rep 2022;71(50):1589 – 96. https://doi.org/10.15585/mmwr.mm7150a4.

SUPPLEMENTARY MATERIAL

Supplementary File 1: The definition of influenza-like illness (ILI), acute respiratory infection (ARI), and severe acute respiratory infection (SARI)

(1) Influenza-like illness (ILI) is a non-specific syndrome defined as fever (temperature of 38 °C or greater) with cough or sore throat. (National Guideline for Institutional Outbreak Management of Seasonal Influenza, 2018 version)

(2) An acute respiratory infection (ARI) is defined as a measured fever of ≥38 °C and cough, with onset within the last 10 days. (The World Health Organization (WHO) Global Influenza Programme, https://www.who.int/teams/global-influenza-programme/surveillance-and-monitoring/case-definitions-for-ili-and-sari)

(3) Severe acute respiratory infection (SARI) is defined as ARI with symptoms including cough and fever within 10 days of presentation and with hospitalization. [The World Health Organization (WHO) Global Influenza Programme, https://www.who.int/teams/global-influenza-programme/surveillance-and-monitoring/case-definitions-for-ili-and-sari]

Supplementary File 2: The criteria for the selection of eight hospitals in Zhejiang Province, China, in this study

(1) We selected the representative hospitals in the northern, central, southern, and coastal areas of Zhejiang Province, covering rural and urban areas.

(2) We selected different levels of hospital, including provincial-level tertiary hospitals, municipal hospitals, and county-level hospitals.

(3) We included general hospitals and specialized pediatric hospitals.

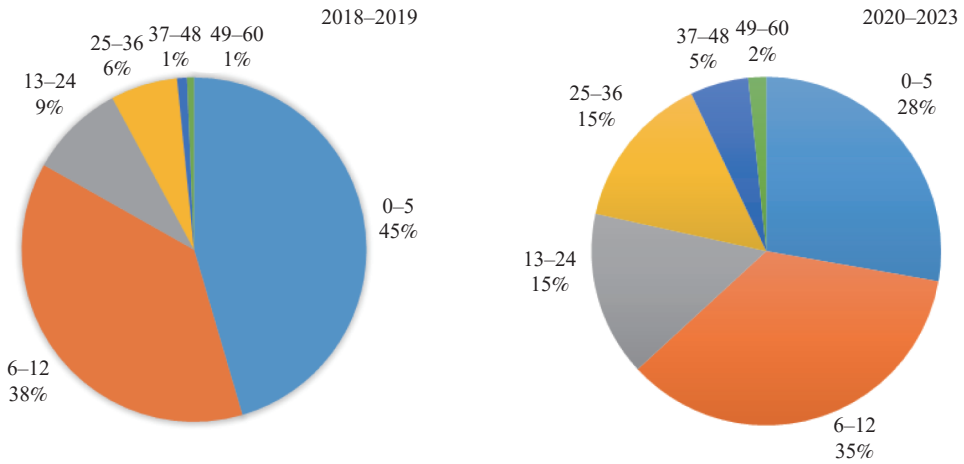

SUPPLEMENTARY FIGURE S1. The age distribution of hospitalized children under 5 years old infected with HRSV in Zhejiang Province, China (pre-pandemic vs. pandemic period).

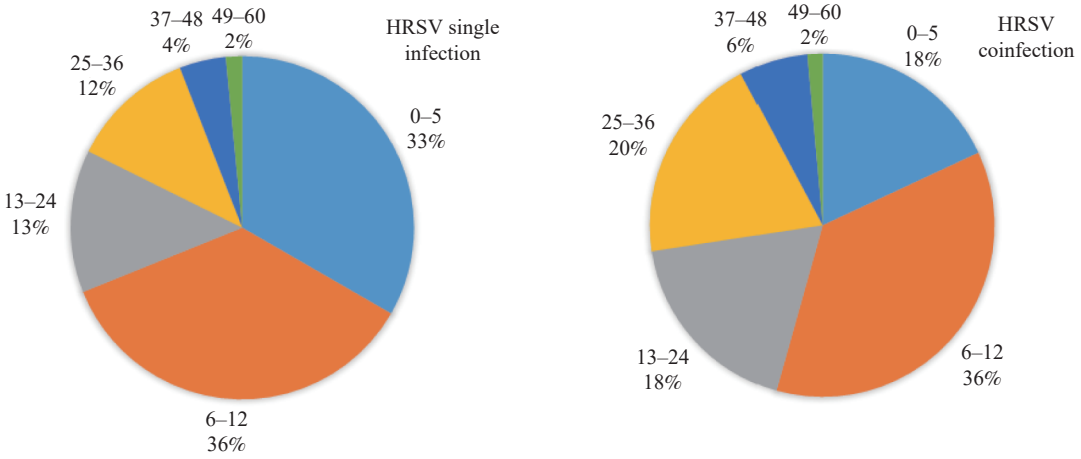

SUPPLEMENTARY FIGURE S2. The age distribution of hospitalized children under 5 years old infected with HRSV alone or coinfected with HRSV in Zhejiang Province, China.

SUPPLEMENTARY TABLE S1. The characteristics of eight hospitals in five prefecture-level cities of Zhejiang Province, China.

Number	Hospital name	Hospital level	Hospital classification	Locations
1	Jiaxing Maternity and Child Health Care Hospital	Level III Grade A	Women and children	Jiaxing City
2	The First Hospital of Jiaxing	Level III Grade A	Comprehensive hospital	Jiaxing City
3	The Second People's Hospital of Jinyun	Level II Grade B	Comprehensive hospital	Lishui City
4	The Maternity and Child Health Hospital of Tonglu	Level II Grade B	Comprehensive hospital	Hangzhou City
5	The First People's Hospital of Tonglu	Level II Grade A	Comprehensive hospital	Hangzhou City
6	Wenzhou Medical College Affiliated Second Hospital Wenzhou Medical College Affiliated Yuying Children's Hospital	Level III Grade A	Women and children	Wenzhou City
7	People's Hospital of Daishan	Level II Grade A	Comprehensive hospital	Zhoushan City
8	Zhoushan Hospital	Level III Grade A	Comprehensive hospital	Zhoushan City

Preplanned Studies

Global Species/Biovars and Genotype Diversity Atlas of *Brucella* spp. — 102 Countries, 1923–2020

Zhiguo Liu[1,&]; Liping Gao[2,&]; Miao Wang[3]; Songnan Du[4]; Min Yuan[1]; Zhenjun Li[1,5,6,#]

Summary

What is already known about this topic?

Brucella spp. are facultative intracellular bacteria that can infect many species of animals and humans.

What is added by this report?

The global *Brucella* demonstrates distinct territorial distribution patterns: *B. abortus* predominantly in Africa and North America, *B. melitensis* dominates in Asia and Europe, and *B. suis* is most prevalent in Europe. *B. melitensis* exhibits the highest host and genotype diversity, with most strains isolated from human cases, indicating persistent animal reservoirs and repeated human transmission. *Brucella* spp. demonstrates region-specific lineage distributions: African *B. abortus* strains cluster within abortus B lineage, while Asian, American, and European strains group within abortus C. Eastern Mediterranean *B. melitensis* strains show predominant distribution across Asia and Europe, while *B. suis* strains display genetic heterogeneity across different geographical regions.

What are the implications for public health practice?

While *B. melitensis* represents a global public health challenge, *B. abortus* and *B. suis* pose more localized concerns. Implementation of livestock brucellosis control programs is essential for reducing human health risks.

Brucellosis represents a globally prevalent zoonotic disease that poses significant public health challenges and causes substantial economic losses in livestock populations (*1*). The past few decades has witnessed continuous expansion in recognized diversity within the *Brucella* genus, with novel strains isolated from marine mammals to ocean fish revealing previously unknown ecological niches (*2*). These developments present new challenges for both regional and global surveillance and control of brucellosis. However, global species/biovars and genotype diversity atlas of *Brucella* spp. remain unclear. Therefore, this study aims to elucidate the global distribution patterns of species/biovars and genetic diversity among *Brucella* strains to enhance understanding of epidemiological changes and facilitate tailored surveillance and control strategies worldwide.

In this study, 7,212 *Brucella* strains collected from multiple locus variable-number tandem repeat analysis (MLVA) databases (https://microbesgenotyping.i2bc.paris-saclay.fr/databases) through June 30, 2024, representing isolates collected in 102 countries from 1923 to 2020. Data extraction included species/biovar, isolation location, quantity, host spectrum, panel 1 profiles, MLVA-11 patterns, lineage information, and isolation dates. Data analysis was performed using Excel 2021 software (Microsoft, Redmond, WA, USA). The minimum spanning tree (MST) was constructed using PHYLOVIZ 2.0 (*3*) online software (https://online2.phyloviz.net/index) to elucidate genetic relationships among strains.

Among the 7,212 *Brucella* strains analyzed, at least 12 species, 19 biovars, and several atypical *Brucella* species were identified (Figure 1). *B. abortus* strains distributed across 59 countries (regions) spanning six continents, while *B. melitensis* exhibited widespread presence in 64 countries throughout Asia, Europe, and North Africa (Figure 1). Notably, the distribution pattern of *B. melitensis* correlates strongly with regions reporting high incidence rates of brucellosis in both humans and animals. *B. suis* strains were documented in 34 countries across Europe, North America, and Latin America. *B. canis* demonstrated a more limited geographic range, primarily concentrated in East Asia and Latin America (Figure 1). Other species showed distinct regional patterns: *B. neotomae* in North America; *B. ovis* in Europe, North Africa, Oceania, and Latin America; *B. ceti* predominantly in West Europe and North America; *B. microti* concentrated in Middle Europe; *B. papionis* restricted to Tanzania and USA; *B. vulpis* exclusively in Austria; and *B. pinnip* primarily in Europe (Figure 1). These distribution patterns indicate the global predominance of *B. abortus* and *B. melitensis*, while other species exhibit distinct geographic specificities.

Continents	*Brucella abortus*	*Brucella melitensis*	*Brucella suis*	*Brucella canis*	*Brucella ceti*	*Brucella microti*	*Brucella neotomae*	*Brucella ovis*	*Brucella papionis*	*Brucella vulpis*	*Brucella pinnip*	*Brucella ama*
Asia	619	3,051	156	12	0	0	0	0	0	0	0	0
Europe	458	1,775	510	5	61	13	0	12	0	1	58	0
Africa	1,265	247	14	3	0	0	0	31	1	0	0	0
Oceania	3	0	11	0	0	0	0	5	0	0	0	0
North America	156	19	8	11	49	0	13	4	1	0	2	2
Latin America	35	121	27	106	0	0	0	129	0	0	0	2

FIGURE 1. Territory distribution of *Brucella* spp. Strains.
Note: The number of strains marked with different color scales; green: refers to the continent with no strains found; red: indicates the continent with the most strains.

The predominant species was *B. melitensis* (*n*=4,042, 56.05%), followed by *B. abortus* (*n*=2,600), *B. suis* (*n*=695), and *B. canis* (*n*=52) (Supplementary Table S1). The geographic distribution of *B. abortus* biovars showed distinct patterns, for example: biovar 1 was predominantly found in Portugal, South Korea, and Brazil; and biovar 9 in Xinjiang, China. Within the *B. melitensis* population, biovar 3 (*n*=1,909) was dominated species. *B. melitensis* biovars 1 and 3 showed widespread distribution across Asia and Europe, particularly in Asian countries with high brucellosis prevalence.

The *B. suis* population exhibited distinct biovar distributions, such as *B. suis* biovar 1 showed broad geographic distribution across China, the USA, Mexico, France, Zimbabwe, Egypt, and Australia. *B. ovis* (*n*=53) was distributed across France, Spain, Brazil, Greece, the USA, Australia, New Zealand, Croatia, and Argentina. *B. neotomae* (*n*=13) was confined to Costa Rica and the USA. Among non-classical species, there were 173 *B. ceti* isolates, 61 *B. pinnipedialis* isolates, 13 *B. microti* isolates, 2 *B. papionis* isolates, and 1 *B. vulpis* isolate. *B. ceti* was predominantly found in Scotland, Italy, Spain, Costa Rica, Germany, France, and the UK. *B. microti* was isolated from the Czech Republic and Austria, *B. papionis* from Tanzania and the USA, and *B. pinnipedialis* from Scotland, Norway, United Kingdom, and USA.

Asia exhibits the lowest species diversity, with *B. abortus* and *B. melitensis* being the only classical species distributed across all Asian countries (Figure 2). Sporadic cases of *B. suis* have been documented in China, India, Nepal, Palestine, and the United Arab Emirates, while *B. canis* has been reported exclusively in China, Republic of Korea, and Japan. This species distribution profile aligns precisely with the regions reporting the highest human brucellosis burden in Asia. Notably, substantial isolations of *B. melitensis* have been recorded in China, Kazakhstan, Kyrgyzstan, Palestine, Qatar, and Turkey - countries that consistently report among the highest global incidence rates of brucellosis.

Europe demonstrates higher species diversity than other continents, with 9 of the 12 known species documented (Figure 2). Three species (*B. abortus, B. melitensis,* and *B. suis*) are widely distributed across the continent, particularly in historically high-burden regions. *B. suis* exhibits a unique continental distribution pattern, with significant presence in Hungary, Germany, Belgium, France, Croatia, Spain, and Portugal, predominantly isolated from swine and wild boar populations. These findings suggest that despite successful control of brucellosis in Europe's historically endemic areas, continued surveillance remains essential.

Despite Africa being a historically endemic region for brucellosis, comprehensive data on *Brucella* species and genotypes remain limited due to insufficient surveillance in recent decades. *B. abortus* strains are particularly prevalent throughout South and West Africa (Figure 2). In Africa presence of multiple *Brucella* species, underscoring the need for expanded bacteriological surveillance.

While Oceania maintains brucellosis-free status with only sporadic isolations of *B. abortus*, *B. suis*, and *B. ovis* (Figure 2), potential public health risks persist through mammalian reservoirs. The Americas exhibit the highest *Brucella* species diversity globally, with at least 10 documented species, and *B. abortus* showing the widest geographic distribution (Figure 2). *B. melitensis* has been documented in regions with substantial human brucellosis burden, including the USA, Mexico, Peru, and Argentina. The continent harbors the highest concentrations of both *B. neotomae* (11 isolates in the USA) and *B. ovis* (115 isolates in Argentina), while Costa Rica reports the majority of *B. ceti* cases.

The *B. abortus* population demonstrates remarkable host diversity, with isolates from at least 20 different species. Cattle represent the primary host (*n*=1,567), followed by bison (*n*=97) and humans (n=80). *B. melitensis* exhibits even greater host diversity, with

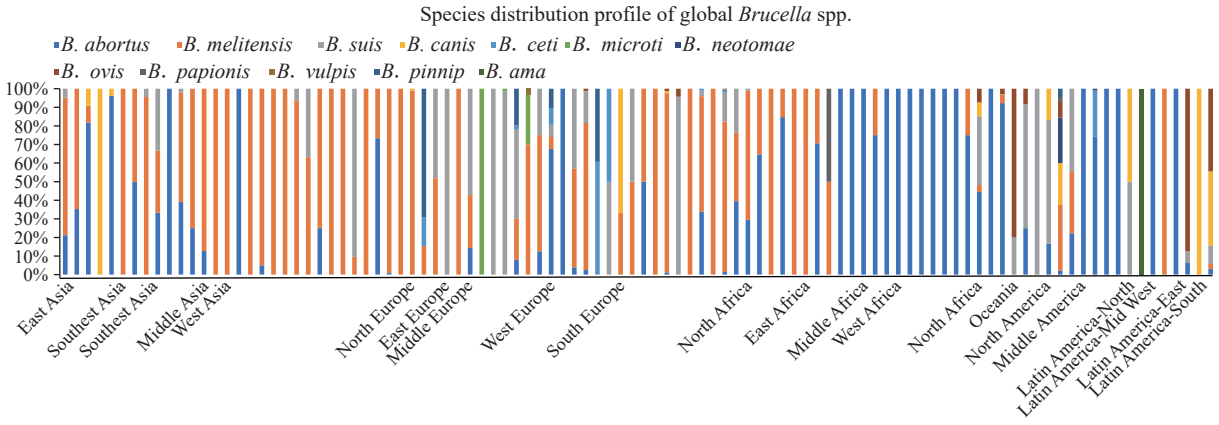

FIGURE 2. Distribution of areas and composition patterns of *Brucella* species populations.
Note: *Brucella* species are coded with color, and dots on the x-axis indicate the borders of different areas.

isolations from 24 distinct species, predominantly humans (*n*=2,719), followed by ovines (*n*=617) and cattle (*n*=280). The *B. suis* population spans 15 host species, *B. neotomae* has been isolated from both rodents and humans. Host specificity is observed in several species, such as *B. papionis* in baboons. This extensive host diversity plays a crucial role in maintaining and facilitating the transmission of *Brucella* strains.

Within the *B. abortus* population, 83 multiple locus variable-number tandem repeat analysis-11 genotypes (GTs) were identified, with three GTs (82, 72, and 79) emerging as predominant, representing 28.4% (494/1,735), 22.4% (390/1,735), and 10.7% (187/1,735) of the population, respectively (Figure 3A). GT72 exhibited broad geographic distribution across 17 countries, GT82 was detected in 10 countries across 3 continents, GT79 was identified in 9 countries across 4 continents.

Minimum spanning tree (MST) analysis based on MLVA-16 data revealed that the *B. abortus* population segregated into two distinct groups (B and C) (Figure 3B), with African strains clustering in abortus B, while strains from Asia, the Americas, and Europe were predominantly found in abortus C (Figure 3B). Within C I, identical MLVA-16 genotypes were shared among strains from the USA, Costa Rica, Kazakhstan, Italy, and Portugal (Figure 3B). In C II, the majority of shared MLVA-16 genotypes were observed between strains from the USA and Portugal, USA and Brazil, and Bangladesh and Brazil (Figure 3B).

Within the *B. melitensis*, 216 MLVA-11 genotypes were identified, with five predominant genotypes (GTs): 116, 96, 125, 111, and 87, accounting for 54.4% (2,733/5,019), 7.1% (360/5,019), 6.1% (307/5,019), 3.6% (182/5,019), and 2.2% (112/5,019), respectively (Figure 4A). GT116 was distributed across at least 18 countries, GT96 was identified in nine countries, GT125 was present in 20 countries.

Minimum spanning tree analysis revealed that the *B. melitensis* clustered into three distinct lineages: Eastern Mediterranean, Western Mediterranean, and Americas (Figure 4B). The Eastern Mediterranean strains predominated in Asia and Europe; the Western Mediterranean lineage comprised strains from Italy, France, Egypt, and Algeria; The American lineage encompassed strains from the USA, Peru, Spain, and Portugal (Figure 4B). Among the three lineages, the Eastern Mediterranean exhibited the highest frequency of shared MLVA-16 genotypes (Figure 4B).

In the *B. suis* population, analysis revealed 67 distinct MLVA-11 genotypes, with five dominant circulating genotypes: GT33 (22.2%, 126/592), GT58 (12.6%, 75/592), GT57 (9.2%, 55/592), GT60 (7.9%, 47/592), and GT44 (7.7%, 46/592) (Figure 5A).

Minimum spanning tree analysis demonstrated that *B. suis* strains clustered into two major lineages (SI and SII), with SI further subdividing into three distinct sub-clades (a–c) (Figure 5B). Notably, shared MLVA-16 genotypes were observed in SI sub-clade b (Figure 5B), while in SII, a single shared MLVA-16 genotype was identified (Figure 5B).

DISCUSSION

Brucella strains exhibit widespread distribution across six continents, the extensive spread and dispersal of these pathogens has been facilitated by frequent

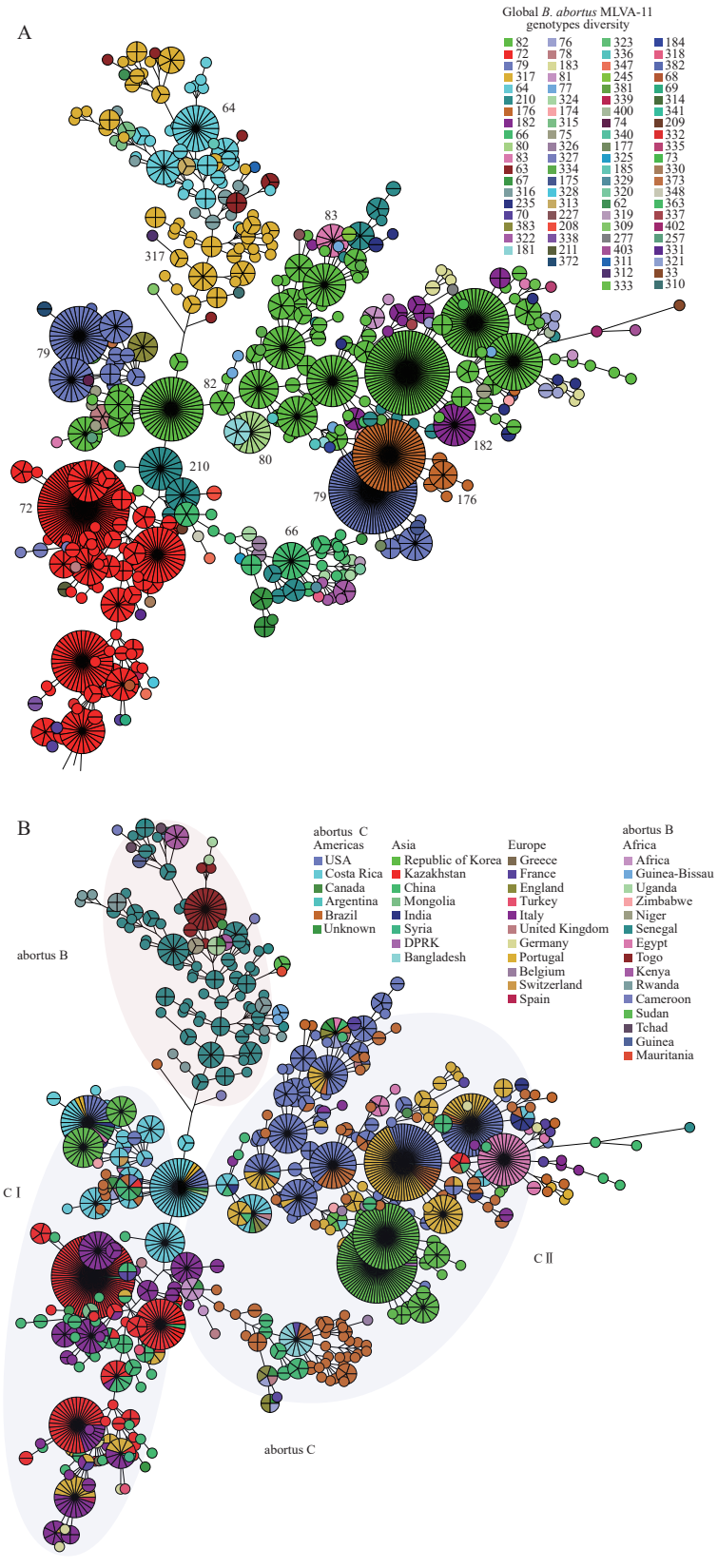

FIGURE 3. MLVA-11 genotype diversity (A) and MLVA-16 genetic relationship (B) of global *B. abortus* strains.
Note: (A) Color marks the MLVA-11 genotypes; numbers in the figure indicate the dominant genotypes; (B) Color-coded countries in which strains isolated from all *B. abortus* strains were divided into two lineages (abortus A and abortus B), and abortus B were further sorted into C I and C II subgroups.

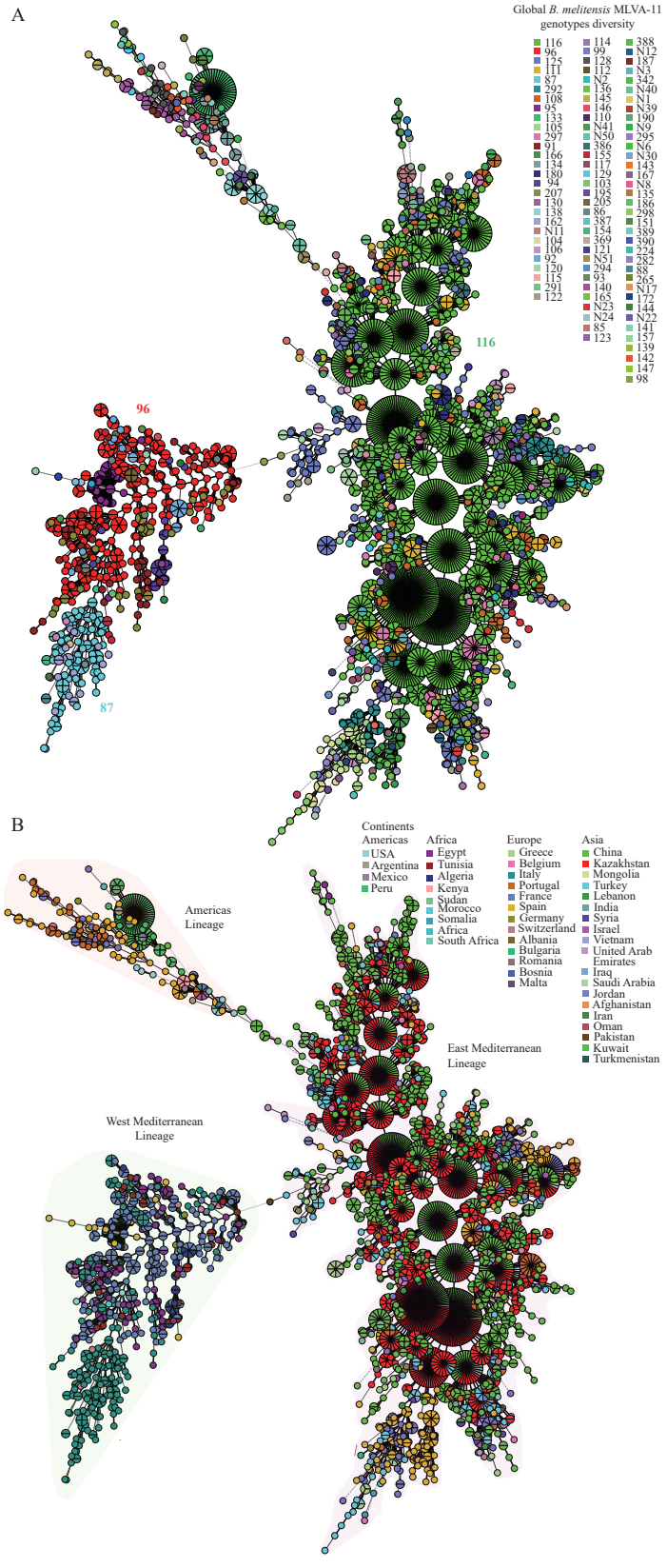

FIGURE 4. MLVA-11 genotypes diversity (A) and MLVA-16 genetic relationships (B) of global *B. melitensis* strains.
Note: (A) Color marks the MLVA-11 genotypes; numbers in the figure indicate the dominant genotypes. (B) Color-coded countries in which strains were isolated; all *B. melitensis* strains were divided into three lineages: East Mediterranean, West Mediterranean, and Americas.

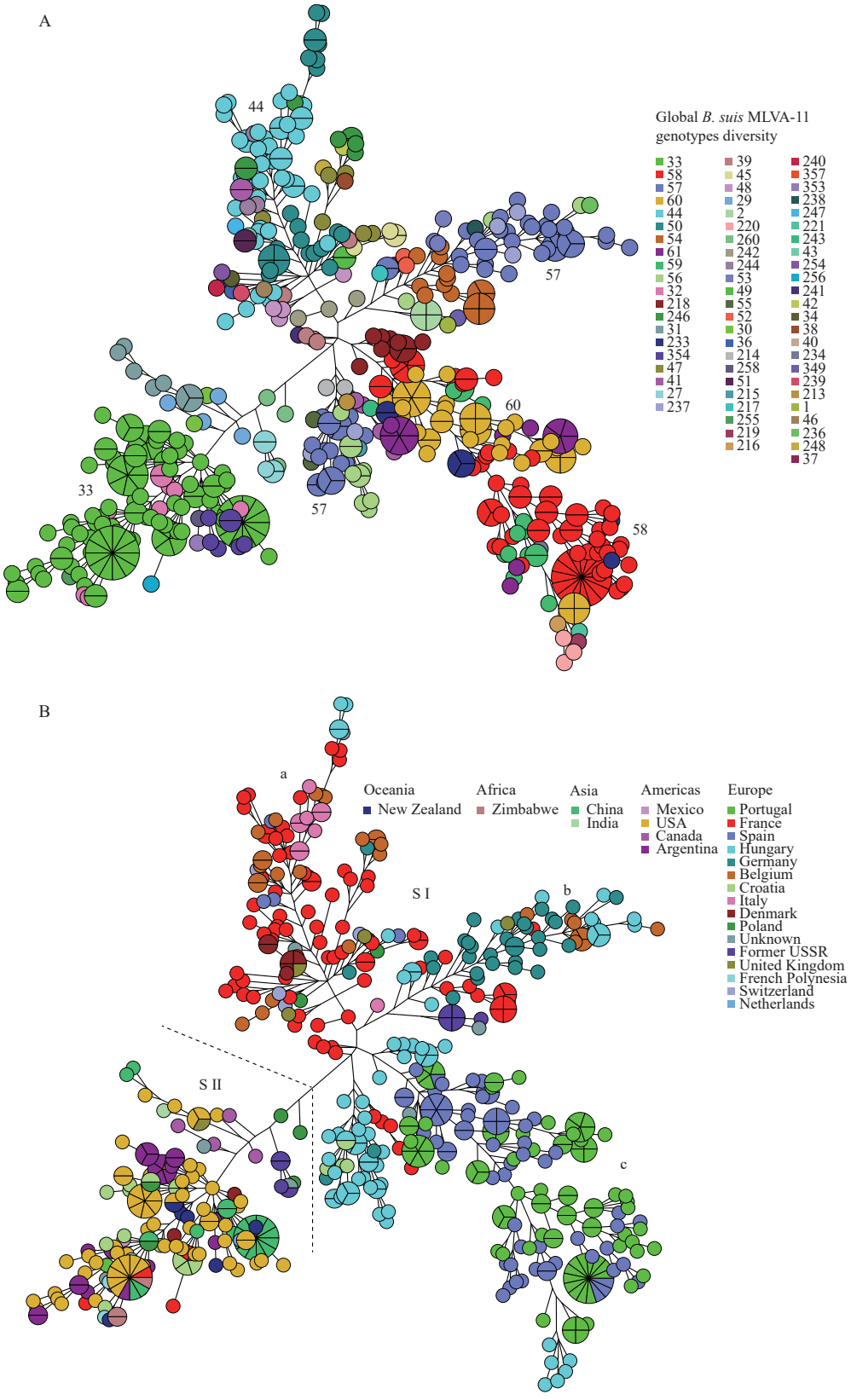

FIGURE 5. MLVA-11 genotype diversity (A) and MLVA-16 genetic relationships (B) of global *B. suis* strains.
Note: (A) Color marks the MLVA-11 genotypes; numbers in the figure indicate the dominant genotypes; (B) Color-coded countries in which strains were isolated; all *B. suis* strains were divided into two lineages (S I and S II), and further S I was further sorted into three subgroups (a-c).

livestock exchange and trade (*4*). The paucity of comprehensive surveys and research in Africa presents a significant obstacle to understanding the disease. Consequently, successful prevention, control, and eradication of brucellosis in low-income countries necessitates substantial financial support, unwavering commitment, and sustained long-term programs. The expanding host spectrum of the *Brucella* spp. population is a critical factor in its ecological persistence and maintenance. Active spillover between domestic animals and wildlife is increasingly recognized as a potential source of human infection. While *Brucella* spp. occasionally colonize non-preferred hosts, there remains high potential for discovering additional ecologically significant natural hosts (*5*).

Global phylogenomic analysis reveals an African origin for *B. abortus*, with subsequent spread to the Middle East, Europe, and Asia, likely facilitated by infected cattle movement (*6*). *B. abortus* strains from Kazakhstan and Russia show genetic relationships with Portuguese, Brazilian, and US isolates, suggesting ancient lineage dispersal from Europe westward to South America and eastward to Turkey, Russia, and Asia (*7*).

The *B. melitensis* population exhibits the highest genetic diversity, with particularly significant genetic homogeneity observed within the E. Mediterranean lineage, especially among Asian strains. All Asian strains clustering into genotype II alongside SEA strains (*8*). the spread of *B. melitensis* subgenotype IIi from Central Asian countries to Russia likely occurred via the northern route of the Great Silk Road, which connected eastern countries with Northern Europe (*9*). The global trade and movement of ruminants has facilitated the spread and dispersal of *B. melitensis*, necessitating stricter regulations on animal transfers from high-epidemic areas and enhanced cross-border inspection and quarantine protocols.

B. suis strains exhibit significant genetic heterogeneity across different global territories. The maintenance and spread of *B. suis* biovar 2 in Europe represents a dynamic process linked to natural wild boar expansion as the primary wild reservoir, while long-distance transmission largely depends on human activities (*10*). Surveillance and control measures in endemic European and Asian regions are essential to accurately assess its public health risk.

This study provides novel insights into the global species/biovars, host spectrum, and genetic diversity of *Brucella* spp. However, several limitations warrant consideration. First, our reliance on international MLVA database data may present an incomplete distribution overview, necessitating further investigation. Second, the complex transmission dynamics of brucellosis demand more nuanced analysis of the interplay between human behavior, environmental factors, and microbial genetics in disease transmission.

The global distribution of *Brucella* species exhibits remarkable genetic and phenotypic diversity, characterized by extensive host range adaptation and broad territorial spread, presenting significant challenges for worldwide surveillance and control efforts. A critical impediment to effective brucellosis management in low-income countries remains the limited allocation of governmental and regional resources. These findings emphasize the urgent need to establish a comprehensive global pathogen surveillance system and molecular tracking network platform to elucidate the composition of circulating *Brucella* strains and understand the global transmission patterns of brucellosis.

Conflicts of interest: No conflicts of interest.

Acknowledgments: All researchers who have previously published data on the isolation, identification, and molecular characterization of *Brucella* spp. worldwide. The developers and administrators of the international *Brucella* MLVAbank genotyping databases (Brucella v4_6_5).

Funding: Supported by the National Key Research and Development Program of China (No. 2021YF2301105). The funding agency had no role in study design, data collection and analysis, publication decisions, or manuscript preparation..

doi: 10.46234/ccdcw2025.023

[#] Corresponding author: Zhenjun Li, lizhenjun@icdc.cn.

[1] National Key Laboratory of Intelligent Tracking and Forecasting for Infectious Diseases, National Institute for Communicable Disease Control and Prevention, Chinese Center for Disease Control and Prevention, Beijing, China; [2] National Key Laboratory of Intelligent Tracking and Forecasting for Infectious Diseases, National Institute for Viral Disease Control and Prevention, Chinese Center for Disease Control and Prevention, Beijing, China; [3] Ulanqab Center for Disease Control and Prevention, Jining City, Inner Mongolia Autonomous Region, China; [4] Tongliao Center for Disease Control and Prevention, Horqin District, Inner Mongolia Autonomous Region, China; [5] Chinese Center for Disease Control and Prevention, Beijing, China; [6] Changzhi Medical College, Changzhi City, Shanxi Province, China.
[&] Joint first authors.

Submitted: September 20, 2024
Accepted: December 03, 2024
Issued: January 24, 2025

REFERENCES

1. Bundle DR, McGiven J. Brucellosis: improved diagnostics and vaccine insights from synthetic glycans. Acc Chem Res 2017;50(12):2958 – 67. https://doi.org/10.1021/acs.accounts.7b00445.
2. Whatmore AM, Foster JT. Emerging diversity and ongoing expansion of the genus *Brucella*. Infect Genet Evol 2021;92:104865. https://doi.org/10.1016/j.meegid.2021.104865.
3. Nascimento M, Sousa A, Ramirez M, Francisco AP, Carriço JA, Vaz C. PHYLOViZ 2. 0: providing scalable data integration and visualization for multiple phylogenetic inference methods. Bioinformatics 2017;33 (1):128 – 9. https://doi.org/10.1093/bioinformatics/btw582.
4. Leylabadlo HE, Bialvaei AZ, Samadi Kafil H. Brucellosis in Iran: why not eradicated? Clin Infect Dis 2015;61(10):1629-30. http://dx.doi.org/10.1093/cid/civ646.
5. Pappas G. The changing *Brucella* ecology: novel reservoirs, new threats. Int J Antimicrob Agents 2010;36 Suppl 1:S8-11. http://dx.doi.org/10.1016/j.ijantimicag.2010.06.013.
6. Janke NR, Williamson CHD, Drees KP, Suárez-Esquivel M, Allen AR, Ladner JT, et al. Global phylogenomic diversity of *Brucella abortus*: spread of a dominant lineage. Front Microbiol 2023;14:1287046. https://doi.org/10.3389/fmicb.2023.1287046.
7. Daugaliyeva A, Sultanov A, Usserbayev B, Baramova S, Modesto P, Adambayeva A, et al. Genotyping of *Brucella melitensis* and *Brucella abortus* strains in Kazakhstan using MLVA-15. Infect Genet Evol 2018;58:135 – 44. https://doi.org/10.1016/j.meegid.2017.12.022.
8. Tan KK, Tan YC, Chang LY, Lee KW, Nore SS, Yee WY, et al. Full genome SNP-based phylogenetic analysis reveals the origin and global spread of *Brucella melitensis*. BMC Genomics 2015;16(1):93. https://doi.org/10.1186/s12864-015-1294-x.
9. Pisarenko SV, Kovalev DA, Volynkina AS, Ponomarenko DG, Rusanova DV, Zharinova NV, et al. Global evolution and phylogeography of *Brucella melitensis* strains. BMC Genomics 2018;19 (1):353. https://doi.org/10.1186/s12864-018-4762-2.
10. Muñoz PM, Mick V, Sacchini L, Janowicz A, de Miguel MJ, Cherfa MA, et al. Phylogeography and epidemiology of *Brucella suis* biovar 2 in wildlife and domestic swine. Vet Microbiol 2019;233:68 – 77. https://doi.org/10.1016/j.vetmic.2019.04.025.

Methods and Applications

Automatic Warning Practice of Multi-Source Surveillance and Multi-Point Trigger for Infectious Diseases — Yuhang District, Hangzhou City, Zhejiang Province, China, January–April 2024

Qinbao Lu[1]; Tianying Fu[1]; Haocheng Wu[1]; Zheyuan Ding[1]; Chen Wu[1]; Weiqun Gan[2,#]; Junfen Lin[1,3,#]

ABSTRACT

Introduction: This study presents empirical evidence from the implementation of an automated infectious disease warning system utilizing multi-source surveillance and multi-point triggers in Yuhang District, Hangzhou City, Zhejiang Province, so as to provide reference for more extensive practice of infectious disease surveillance and early warning in the future.

Methods: The data were obtained from the Health Emergency Intelligent Control Platform of Yuhang District from January 1 to April 30, 2024, encompassing warning signal issuance and response documentation. Descriptive epidemiological method was used to analyze the early warning signals.

Results: From January 1 to April 30, 2024, the Health Emergency Intelligent Control Platform in Yuhang District generated 4,598 valid warning signals, with a warning signal positive rate of 36.43%. The early warning system detected 71 infectious disease outbreaks reported through the Intelligent Control Platform, including 24 single-source early warning and 47 multi-source early warning. The sensitivity was 78.02%, demonstrating improved performance compared to existing infectious disease surveillance and warning systems.

Conclusions: This represents the first domestic publication evaluating an automated multi-source surveillance and multi-point trigger warning system. By integrating and correlating multi-source data, the system can efficiently and accurately detect warning signals of infectious disease incidents, which has significant practical implications for early surveillance, warning, and management of infectious diseases.

Infectious diseases remain a persistent global health threat. The increasing impact of emerging and re-emerging infectious diseases in recent years has created unprecedented challenges for disease surveillance and warning systems (*1*). The development of intelligent warning mechanisms incorporating multi-point triggers and multi-channel surveillance represents a crucial advancement in enhancing early detection and warning capabilities for infectious diseases (*2–3*).

Building upon theoretical research in intelligent warning system development, Yuhang District has implemented a Health Emergency Intelligent Control Platform. This comprehensive system integrates data management, warning triggers, emergency command operations, and visual analytics capabilities. The platform facilitates sophisticated disease surveillance through multiple data sources, employs diverse analytical models, and implements multi-point warning triggers. Through coordinated command and control mechanisms, the platform enables rapid information dissemination and emergency response deployment.

Yuhang District, situated in northwestern Hangzhou City, Zhejiang Province, encompasses 942 km^2 and comprises 5 towns and 7 sub-districts. As of 2023, the district's population has reached 1.36 million. This study presents an analysis of surveillance and warning outcomes from the Health Emergency Intelligent Control Platform implemented in Yuhang District.

METHODS

Data Sources

The data were obtained from the Health Emergency Intelligent Control Platform of Yuhang District from January 1 to April 30, 2024, encompassing warning signal issuance and response documentation. The multi-source surveillance system integrates three primary data streams: syndromic data from the hospital

information system (HIS) of medical institutions, school illness-related absenteeism records, and infectious disease report cards. The HIS data comprises patient demographics, syndromic presentations, diagnostic information, disease onset timing, and consultation dates. School absenteeism records include student demographics, specific absence justifications, and absence dates. Infectious disease report cards contain case demographics, disease onset timing, diagnostic classifications, reporting timestamps, and reporting institution identifiers.

Warning Process

The platform synthesizes these multi-source data streams through integrated algorithmic models to implement hierarchical surveillance and warning protocols. The system achieves multidimensional warning capabilities by correlating surveillance data across multiple domains, including student enrollment records and elderly care facility resident identification data. The warning mechanism primarily employs fixed-value algorithms for rapid alert generation. Upon warning signal activation, the system automatically notifies the relevant local community health service center. Healthcare staff then process the incident through a dedicated management system, ensuring comprehensive closed-loop operational oversight.

Analysis Indicators and Definitions

This study analyzes warning signal frequencies and their corresponding response outcomes. Signal verification was conducted through data analysis and telephone verification protocols. The following key metrics were evaluated: 1) Positive warning signals, defined as signals that, upon verification, indicated early manifestation of an infectious disease outbreak; 2) Positive warning signal rate, calculated as the percentage of positive warning signals among valid warning signals; and 3) Warning sensitivity, measured as the proportion of actual outbreak incidents successfully identified by the warning system. To validate the warning platform's sensitivity, this study utilized clustered infectious disease incidents reported through the district's intelligent control platform as the reference standard for actual outbreak incidents.

Statistical Analysis

Data organization and analysis were performed using WPS Excel 2016 software (Kingsoft, Beijing, China). Chi-square tests for positive rates were conducted using R software (version 4.4.1; The R Foundation for Statistical Computing, Vienne, Austria), with $P<0.05$ considered statistically significant.

RESULTS

Basic Situation

From January 1 to April 30, 2024, the Health Emergency Intelligent Control Platform in Yuhang District generated 5,944 warning signals. After excluding 1,346 duplicate signals, 4,598 valid warning signals remained, averaging 38 valid signals per day. Following data analysis and telephone verification, 1,184 signals were eliminated, yielding 3,414 preliminary suspected signals. These comprised 2,663 single-source triggers, 318 two-source triggers, and 433 three-source triggers.

Positive Rate of Warning Signals

Investigation confirmed 1,675 positive warning signals, representing 36.43% (1,675/4,598) of valid signals. The positive rates varied by data source: HIS system syndromes at 32.44% (1,367/4,214), illness-related absenteeism at 78.93% (251/318), and infectious disease report cards at 86.36% (57/66). Chi-square analysis revealed statistically significant differences among these three sources ($\chi^2=348.073$, $P<0.001$), as shown in Table 1. Of the 2,923 false positive signals, 2,564 (87.72%) were attributed to angina syndrome, which primarily represented non-communicable conditions such as acute angina and laryngopharyngitis. After excluding these angina syndrome false positives, the HIS system's syndrome warning positive rate increased to 82.85% (1,367/1,650), and the overall valid positive rate reached 82.35% (1,675/2,034). This adjusted analysis showed no statistically significant differences in positive rates among HIS system syndromes, school absenteeism, and infectious disease report cards ($\chi^2=3.571$, $P=0.168$).

Of the 1,675 positive warning signals, HIS system syndromes constituted the majority at 81.61%, with fever respiratory syndromes being predominant (62.69%). Angina syndrome signals accounted for 16.72% (280 signals). School absenteeism due to illness generated 251 positive warning signals (14.99%), primarily from fever symptoms (8.42%). The infectious disease report cards yielded 57 positive warning signals (3.40%), with mumps representing 98.25% (56/57) of these cases (Table 2).

TABLE 1. Results of multi-source surveillance and multi-point trigger warning in Yuhang District, Hangzhou City.

Data source	Number of valid signals	Number of positive signals	Positive rate (%)
HIS system syndromes	4,214	1,367	32.44
School absenteeism due to illness	318	251	78.93
Infectious disease report cards	66	57	86.36
Total	4,598	1,675	36.43

TABLE 2. Composition and positive signals of multi-source surveillance and multi-point trigger early warning.

Warning category		Number of positive signals	Composition ratio (%)
HIS system syndromes	Fever Respiratory	1,050	62.69
	Angina	280	16.72
	Gastroenteritis	21	1.25
	Mumps	15	0.90
	Fever with Rash	1	0.06
	Subtotal	1,367	81.61
School absenteeism due to illness	Fever	141	8.42
	Cough/Sore Throat/Runny Nose	64	3.82
	Fever, Cough/Sore Throat/Runny Nose	40	2.39
	Nausea/Vomiting/Diarrhea	6	0.36
	Subtotal	251	14.99
Infectious disease report cards	Mumps	56	3.34
	Hand-Foot-and-Mouth Disease	1	0.06
	Subtotal	57	3.40
Total		1,675	100.00

Abbreviation: HIS=hospital information system.

Warning Sensitivity

From January to April 2024, the multi-point trigger warning system detected 71 out of 91 infectious disease outbreaks reported through the Intelligent Control Platform, yielding a warning sensitivity of 78.02% (71/91). Multi-source warnings accounted for 66.20% (47 cases) of successful detections, while single-source warnings comprised 33.80% (24 cases). Notably, only 33.80% (24 cases) were detected through infectious disease report cards. Among the 20 undetected incidents, the distribution was: 11 cases of other infectious diarrheal diseases, 5 cases of influenza, and 4 cases of hand-foot-and-mouth disease. Analysis of these missed detections revealed several contributing factors: 11 incidents involved delayed student absenteeism feedback combined with mild symptoms that did not prompt medical visits; 4 incidents had cases dispersed across different classes; 2 incidents lacked complete student enrollment information; 1 incident each was attributed to non-imported infectious disease report card data and treatment at an out-of-jurisdiction medical facility. Additionally, one hand-foot-and-mouth disease incident went undetected due to a warning threshold set above the clustering standard.

DISCUSSION

Analysis of the Yuhang District Health Emergency Intelligent Control Platform's operational data from January to April 2024 demonstrates the effectiveness of its multi-source surveillance and multi-point trigger warning system. The system successfully generated warning signals by integrating data from three primary sources: hospital information system syndromes, infectious disease report cards, and school absenteeism records, with HIS-derived syndromic data serving as the predominant warning trigger.

Our analysis identified 1,346 duplicate warning signals, which were generated sequentially as case numbers increased. While single-source triggers constituted the majority of suspected signals, multi-source triggers were less frequent. This pattern may be attributed to two key factors: first, individuals with mild symptoms often did not seek medical attention,

resulting in incomplete diagnostic data for warning generation; second, gaps in illness-related absenteeism reporting led to missed warning signals from school surveillance data.

The distribution of positive warning signals was predominantly characterized by fever respiratory syndromes, demonstrating this indicator's sensitivity in detecting potential disease transmission risks. However, infectious disease report cards generated relatively few positive signals, limited primarily to mumps and hand-foot-and-mouth disease. This limitation stems from several factors: first, the report cards originate from the China Information System for Disease Control and Prevention (CISDCP), where many cases either lack definitive infectious disease diagnoses or involve non-notifiable conditions; second, the platform has not achieved real-time data integration, requiring manual data transfer from CISDCP; and third, the effectiveness of report card-based warnings depends on accurate diagnosis and standardized reporting practices by healthcare facilities. Consequently, relying solely on infectious disease report cards for warning generation may result in data gaps that compromise the system's sensitivity.

Of the 1,675 warning signals confirmed as early indicators of infectious disease outbreaks, community health service centers implemented timely preventive measures, with only 71 cases requiring on-site management for cluster or outbreak events. The system achieved a valid positive warning rate of 36.43%, which improved to 82.35% after excluding false-positive angina syndrome signals — significantly higher than the China Infectious Diseases Automated-alert and Response System (CIDARS) results in Zhejiang Province from 2014 to 2016 (0.57%) (*4*). After excluding false-positive angina syndrome signals, no statistical differences were observed in positive rates among HIS syndromes, school absenteeism, and infectious disease report cards. Future system optimization will focus on refining angina syndrome criteria to reduce false-positive signals and enhance warning specificity. Notably, the system's sensitivity surpassed the spatiotemporal detection warning results of CIDARS in Zhejiang Province from 2017 to 2021 (66.02%) (*5*). These findings suggest that comprehensive student registration information, combined with integrated multi-source data from absenteeism, medical visits, and disease reports, substantially improves both the positive rate and accuracy of warning signals.

The empirical evidence demonstrates that all 24 single-source warnings originated from infectious disease report cards, while the remaining 47 warnings utilized multiple data sources, including absenteeism records. These findings underscore that multi-point trigger surveillance and warning systems enhance detection sensitivity while reducing omissions caused by human error and procedural inconsistencies (*6*–*7*). Furthermore, the analysis of the 20 undetected incidents highlights critical areas for improvement, including the need for higher-quality surveillance data through comprehensive absenteeism reporting and expanded geographical coverage. Enhancement of warning models, particularly through the integration of fixed-value warnings with model-based approaches, could further optimize warning sensitivity.

The implementation of an automated infectious disease warning system incorporating multi-source surveillance and multi-point triggers enables real-time data integration from critical locations and populations, including medical facilities, educational institutions, and elderly care centers. Through the correlation and integration of diverse data sources, the system efficiently identifies and validates warning signals for infectious disease incidents. This comprehensive approach to warning and incident management encompasses infectious diseases, five syndromic categories, and location-specific surveillance, demonstrating significant practical value for early detection, warning, and disease control measures.

Despite these advances, the platform's multi-source surveillance data coverage remains constrained, primarily relying on syndromic data from healthcare facilities, infectious disease report cards, and school-based symptom surveillance. The platform has not yet achieved complete data integration with infectious disease reporting systems. Additionally, current warning algorithms require further optimization, and the integration of various predictive models needs additional exploration.

Future developments will expand data sources to include pharmacy sales records, laboratory testing data from hospital LIS, nursing home records, and inbound traveler information. Concurrent efforts will focus on optimizing the warning model and enhancing the platform's overall effectiveness.

Conflicts of interest: No conflicts of interest.

Funding: Supported by the Major Science and Technology Project of the Science and Technology Department of Zhejiang Province (2021C03038, 2022C03109) and the Medical and Health Science

and Technology Project of Zhejiang Province (2024KY895, WKJ-ZJ-2522, 2025KY774).

doi: 10.46234/ccdcw2025.022

[#] Corresponding authors: Junfen Lin, jflin@cdc.zj.cn; Weiqun Gan, ganwq@yuhang.gov.cn.

[1] Zhejiang Provincial Center for Disease Control and Prevention, Hangzhou City, Zhejiang Province, China; [2] Yuhang District Center for Disease Control and Prevention (Health Supervision Institute), Hangzhou City, Zhejiang Province, China; [3] Zhejiang Provincial Key Laboratory for Vaccine, Prevention and Control of Infectious Diseases, Hangzhou City, Zhejiang Province, China.

Submitted: November 15, 2024
Accepted: January 12, 2025
Issued: January 24, 2025

REFERENCES

1. Baker RE, Mahmud AS, Miller IF, Rajeev M, Rasambainarivo F, Rice BL, et al. Infectious disease in an era of global change. Nat Rev Microbiol 2022;20(4):193 – 205. https://doi.org/10.1038/s41579-021-00639-z.
2. Yang WZ, Lan YJ, Lv W, Leng ZW, Feng LZ, Lai SJ, et al. Establishment of multi-point trigger and multi-channel surveillance mechanism for intelligent early warning of infectious diseases in China. Chin J Epidemiol 2020;41(11):1753 – 7. https://doi.org/10.3760/cma.j.cn112338-20200722-00972.
3. Fan GH, Zhang T, Lai SJ, Feng LZ, Yang WZ. Progress and challenge in intelligent syndromic surveillance for infectious diseases. Chin J Epidemiol 2023;44(9):1338 – 43. https://doi.org/10.3760/cma.j.cn112338-20230320-00159.
4. Lu QB, Lin JF, Xu XP, Wu C, Wu HC, Ding ZY, et al. Analysis and quality evaluation on monitoring data of automatic alert and response system for infections diseases in Zhejiang Province, 2014-2016. Int J Epidemiol Infect Dis 2018;45(2):93 – 7. https://doi.org/10.3760/cma.j.issn.1673-4149.2018.02.006.
5. Lu QB, Wu HC, Ding ZY, Wang XY, Wu C, Lin JF. Evaluation on the effect of temporal-spatial model for outbreak detection of infectious diseases in Zhejiang province. Pract Prev Med 2024;31(2):152 – 5. https://doi.org/10.3969/j.issn.1006-3110.2024.02.006.
6. Wang JL, Chen T, Ren X, Zhang WW, Han YJ, Wang DY, et al. The exploration of strategy for intelligent surveillance and early warning of important respiratory infectious diseases and application of effective countermeasures. Chin J Virol 2021;37(5):1175 – 8. https://doi.org/10.13242/j.cnki.bingduxuebao.004024.
7. Chinese Government Website. Comprehensive advancement of intelligent multi-point trigger infectious disease surveillance and early warning system construction. 2023. https://www.gov.cn/xinwen/jdzc/202312/content_6922957.htm. [2023-12-28]. (In Chinese).

Notifiable Infectious Diseases Reports

Reported Cases and Deaths of National Notifiable Infectious Diseases — China, November 2024*

Diseases	Cases	Deaths
Plague	0	0
Cholera	0	0
SARS-CoV	0	0
Acquired immune deficiency syndrome†	4,760	1,763
Hepatitis	154,173	495
Hepatitis A	1,036	0
Hepatitis B	133,186	40
Hepatitis C	17,027	454
Hepatitis D	19	0
Hepatitis E	2,421	1
Other hepatitis	484	0
Poliomyelitis	0	0
Human infection with H5N1 virus	0	0
Measles	116	0
Epidemic hemorrhagic fever	777	4
Rabies	18	18
Japanese encephalitis	13	0
Dengue	5,201	0
Anthrax	24	0
Dysentery	2,128	0
Tuberculosis	51,790	238
Typhoid fever and paratyphoid fever	340	0
Meningococcal meningitis	10	2
Pertussis	7,829	0
Diphtheria	0	0
Neonatal tetanus	2	0
Scarlet fever	5,111	0
Brucellosis	3,878	1
Gonorrhea	9,211	0
Syphilis	52,434	2
Leptospirosis	36	0
Schistosomiasis	0	0
Malaria	282	4
Human infection with H7N9 virus	0	0
Monkey pox§	16	0
Influenza	166,917	1
Mumps	8,096	0

Continued

Diseases	Cases	Deaths
Rubella	58	0
Acute hemorrhagic conjunctivitis	1,912	0
Leprosy	14	0
Typhus	175	0
Kala azar	24	0
Echinococcosis	388	0
Filariasis	0	0
Infectious diarrhea[¶]	100,831	0
Hand, foot and mouth disease	58,827	0
Total	635,391	2,528

* According to the National Bureau of Disease Control and Prevention, not included coronavirus disease 2019 (COVID-19).
† The number of deaths of acquired immune deficiency syndrome (AIDS) is the number of all-cause deaths reported in the month by cumulative reported AIDS patients.
§ Since September 20, 2023, Monkey pox was included in the management of Class B infectious diseases.
¶ Infectious diarrhea excludes cholera, dysentery, typhoid fever and paratyphoid fever.
The number of cases and cause-specific deaths refer to data recorded in National Notifiable Disease Reporting System in China, which includes both clinically-diagnosed cases and laboratory-confirmed cases. Only reported cases of the 31 provincial-level administrative divisions in the Chinese mainland are included in the table, whereas data of Hong Kong Special Administrative Region, Macau Special Administrative Region, and Taiwan, China are not included. Monthly statistics are calculated without annual verification, which were usually conducted in February of the next year for de-duplication and verification of reported cases in annual statistics. Therefore, 12-month cases could not be added together directly to calculate the cumulative cases because the individual information might be verified via National Notifiable Disease Reporting System according to information verification or field investigations by local CDCs.

doi: 10.46234/ccdcw2025.024

Submitted: December 19, 2024
Accepted: December 23, 2024
Issued: January 24, 2025

Youth Editorial Board

Indexed by Science Citation Index Expanded (SCIE), Social Sciences Citation Index (SSCI), PubMed Central (PMC), Scopus, Chinese Scientific and Technical Papers and Citations, and Chinese Science Citation Database (CSCD)

The inauguration of *China CDC Weekly* is in part supported by Project for Enhancing International Impact of China STM Journals Category D (PIIJ2-D-04-(2018)) of China Association for Science and Technology (CAST).

CCDC weekly

Vol. 7 No. 4 Jan. 24, 2025

Responsible Authority
National Disease Control and Prevention Administration

Sponsor
Chinese Center for Disease Control and Prevention

Editing and Publishing
China CDC Weekly Editorial Office
No.155 Changbai Road, Changping District, Beijing, China
Tel: 86-10-63150501, 63150701
Email: weekly@chinacdc.cn

CSSN
ISSN 2096-7071 (Print)
ISSN 2096-3101 (Online)
CN 10-1629/R1